Gap junctions deliver malonyl-CoA from soma to germline to support embryogenesis in *Caenorhabditis elegans*

Todd A. Starich[1,2] and David Greenstein[1]

[1]Department of Genetics, Cell Biology and Development, University of Minnesota, Minneapolis, Minnesota 55455 USA

[2]Email: stari001@umn.edu

Abstract

Gap junctions are ubiquitous in metazoans and play critical roles in important biological processes, including electrical conduction and development. Yet, only a few defined molecules passing through gap junction channels have been linked to specific functions. We isolated gap junction channel mutants that reduce coupling between the soma and germ cells in the *C. elegans* gonad. We provide evidence that malonyl-CoA, the rate-limiting substrate for fatty acid synthesis (FAS), is produced in the soma and delivered through gap junctions to the germline; there it is used by fatty acid synthase to critically support embryonic development. Separation of malonyl-CoA production from its site of utilization facilitates somatic control of germline development. Additionally, we demonstrate that loss of malonyl-CoA production in the intestine negatively impacts germline development independently of FAS. Our results suggest that metabolic outsourcing of malonyl-CoA may be a strategy by which the soma communicates nutritional status to the germline.

24 **Impact Statement**

25 Malonyl-CoA, the rate-limiting substrate for fatty acid synthesis, is produced in

26 the soma and delivered through gap junctions to the germline to promote

27 reproduction and coordinate it with nutritional status.

Introduction

Gap junctions are clusters of intercellular channels allowing direct passage of small molecules between coupled cells. They are widespread in multicellular organisms, though different gene families encode the protein subunits in invertebrates (innexins) and vertebrates (primarily connexins) (*Skerrett et al., 2017*). While the capability of small molecules to pass through gap junctions can be shown readily in cultured cells, identification of essential molecules that must pass through channels *in vivo* is challenging. Additionally, disruption of gap junction coupling can affect cell adhesion (*Meyer et al., 1992*), and resultant defects in intercellular communication may not necessarily relate to the passage of molecules through junctional channels.

In *C. elegans*, germ cells are coupled throughout their development to the somatic gonad by gap junctions (*Starich et al., 2014*). Germ cells progress in assembly-line fashion through the early stages of meiosis (*Figure 1A*). Gonadal gap junctions have been implicated in germ cell proliferation, oocyte growth, regulation of oocyte meiotic maturation, early embryogenesis and sperm guidance (*Govindan et al., 2006; Whitten et al., 2007; Nadarajan et al., 2009; Edmonds et al., 2011; Starich et al., 2014*). Gap junction hemichannels (half-channels) in the somatic gonad are comprised of the recently duplicated innexins INX-8 and INX-9; apposing germ cell hemichannels are heteromeric and consist of INX-14 in conjunction with either INX-21 or INX-22 (*Figure 1–figure supplement 1*). Germ cells fail to proliferate in *inx-8(0) inx-9(0)* mutants, at a point

upstream of, or parallel to, GLP-1/Notch activation of germ cells by Delta class ligands LAG-2 and APX-1. These ligands are produced in the distal tip cell (DTC) that maintains the proliferative stem cell niche (*Austin and Kimble, 1987, 1989; Henderson et al., 1994; Nadarajan et al., 2009*).

Germ cell proliferation can be rescued in *inx-8(0) inx-9(0)* mutants to half the level of wild type by driving *inx-8* expression in the DTC with the *lag-2* promoter (*Starich et al., 2014*). In these animals, gap junctions between soma and germline are established in the distal gonad arm, but ostensibly not in the proximal arm; many resultant embryos exhibit characteristics of the Pod phenotype (Polarity and Osmotic sensitivity Defect) (*Tagawa et al., 2001*), including eggshell and permeability barrier deficiencies, cytokinesis failures, and polar body extrusion defects. Other genes with mutations producing Pod embryos include those involved in eggshell synthesis, fatty acid synthesis (FAS), the APC/separase pathway, and a coronin-like protein (*Rappleye et al., 1999, 2003; Tagawa et al., 2001; Zhang et al., 2005; Johnston et al., 2006; Olson et al., 2006; Benenati et al., 2009*).

Molecules moving through soma-germ cell gap junctions necessary for proliferation and early embryogenesis are unknown. We use genetic methods to show that malonyl-CoA (mal-CoA) is produced by *pod-2* (acetyl-CoA carboxylase, ACC) in the soma. Transfer of mal-CoA to the germline, for use by *fasn-1* (fatty acid synthase, FASN), is impacted by the integrity of INX-8-containing channels under conditions in which gap junction formation appears

normal. Rescue of the Pod phenotype in *pod-2* genetic mosaics indicates a somatic sheath focus of action. Our results support the model that mal-CoA transits from soma to germline through gap junction channels.

Results

Gametogenesis is delayed by the *inx-8(tn1513 tn1555)* reduction of function (*rf*) mutation

We previously isolated (in an *inx-9* null background) a strong loss-of-function *inx-8* allele *(tn1513)* with sufficient residual function to contribute to channel formation and cell adhesion but not to support germ cell proliferation (*Starich et al., 2014*). *tn1513* encodes a T239I change in the second extracellular loop of the innexin monomer, predicted to be involved in docking with octameric hemichannels on apposing cells (*Figure 1–figure supplement 1*) (*Oshima et al., 2016*). Using this allele in a genetic screen for restoration of germ cell proliferation, six *inx-8* intragenic suppressor mutations were isolated (to be described elsewhere). One of these, *tn1555*, encodes a D24N change in the amino terminus (*Figure 1–figure supplement 1*), near a site that may associate with a cytoplasmic dome structure surrounding the hemichannel outer pore (*Oshima et al., 2016*). *inx-8(tn1513 tn1555rf)*—for brevity to be referred to as *inx-8(rf)*—partially restored germ cell numbers and fertility to one-third the level of wild type (*Figure 1–figure supplement table 1*). *inx-8(rf)* is rescued by an *inx-8(+)* extrachromosomal array, and rescue of *inx-8(0) inx-9(0)* with an *inx-8(rf)::gfp* array mimics the phenotype of the suppressor mutant; therefore observed phenotypes can be attributed to *inx-8(rf)* and not to other possible background mutations.

97 There is an ~18 hr delay to the onset of fertilization in *inx-8(rf)* compared
98 to wild type, as determined by relating the timing of first ovulation to the L4 molt
99 (L4-to-adult transition) (*Figure 1B*). This delay correlates with late expression of
100 *gfp::lin41* in relation to L4 sub-stages of vulval development (*Mok et al., 2015*);
101 LIN-41 is the earliest known marker of oogenesis (*Spike et al., 2014*). In wild type
102 at 20°C, *gfp::lin41* appears by sub-stage L4.7 (*Figure 1C*); in *inx-8(rf)*, *gfp::lin41*
103 is expressed after completion of vulval morphogenesis but prior to the L4 molt
104 (*Figure 1C; Figure 1–figure supplement table 2*). Spermatogenesis is also
105 delayed—wild-type sperm appear as early as the L4.7 stage, but *inx-8(rf)* sperm
106 first appear after completion of vulval morphogenesis (*Figure 1–figure*
107 *supplement table 2*). Once started, egg-laying in *inx-8(rf)* continues apace such
108 that ~99% of progeny are laid within a 96-hour window (3144/3179 larvae; n=25),
109 similar to wild type (5847/5929 larvae; n=21).
110

111 ***inx-8(rf)* gap junction formation is more severely affected in proximal**
112 **gonad arms**

113 To examine expression of INX-8(T239I D24N) mutant innexins encoded by *inx-*
114 *8(rf)*, specific antibodies were used to label somatic (anti-INX-8) or the two
115 classes of germline (anti-INX-21 or anti-INX-22) hemichannels. In wild-type
116 hermaphrodites, clusters of gap junction puncta form between somatic DTC or
117 sheath cells and each underlying germ cell (*Figure 2A*). In distal arms of wild
118 type, loosely clustered sheath-germ cell gap junctions form more basally on germ

119 cells; in *inx-8(rf)* distal arms, both INX-21 and INX-22 puncta tend to localize
120 more laterally, where the sheath cells dip down between adjacent germ cells
121 (*Figure 2B*). In the loop region (transition from meiotic pachytene to diplotene),
122 large, higher-order clusters of gap junction puncta form in wild-type animals;
123 these are absent in *inx-8(rf)* (*Figure 2C*). In wild-type proximal arms (diakinesis),
124 developing oocytes exhibit extensive formation of INX-22 gap junction puncta,
125 while INX-21 puncta become faint; in *inx-8(rf)* proximal arms, INX-22 and INX-8
126 are strongly but diffusely expressed, with little co-localization evident (*Figure 2D*).
127 These results suggest there may be little gap junction coupling in *inx-8(rf)*
128 proximal arms. We showed previously that sheath-oocyte gap junctions are
129 endocytosed by the oocyte during ovulation (*Starich et al., 2014*). Embryos from
130 *inx-8(0) inx-9(0)* rescued with *inx-8(rf)::gfp* show internalized GFP puncta,
131 confirming that *inx-8(rf)* establishes at least some sheath-oocyte gap junctions in
132 the proximal arm (*Figure 2–figure supplement 1*).
133 Reduced proximal arm expression of gap junctions is seen in *inx-8(0) inx-*
134 *9(0); Ex[lag-2p::inx-8::gfp]* animals—simplified to *inx-8/9(0); Ex[inx-8(DTC+, Sh-*
135 *)]*–which are rescued for germ cell proliferation by driving expression of INX-
136 8::GFP in the DTC, but not sheath (Sh), using the *lag-2* promoter (*Starich et al.,*
137 *2014*). These animals produce primarily dead embryos, many with Pod
138 characteristics (*Table 1*). In contrast to *inx-8(rf)*, these embryos do not show
139 evidence of *inx-8::gfp* endocytosis, consistent with absence of proximal arm
140 sheath-germline gap junction coupling (*Figure 2–figure supplement 1*). *inx-8/9(0);*

141 *Ex[inx-8(DTC+, Sh-)]* animals also show delayed onset of *gfp::lin41* expression,
142 similar to *inx-8(rf)* (*Figure 1C; Figure 1–figure supplement table 2*).
143 We conclude that delayed gametogenesis in *inx-8(rf)* mutants arises from
144 compromised soma-germline gap junction communication, due to altered channel
145 properties that influence the formation and localization of gap junctions,
146 especially in the loop and proximal arm. These regions are additionally implicated
147 because DTC expression of wild-type INX-8 fails to rescue *inx-8(rf)* phenotypes
148 (n>20).
149

150 ***inx-8(rf)* interacts with FAS mutants**

151 Because *inx-8/9(0); Ex[inx-8(DTC+, Sh-)]* produces Pod-like embryos, and *inx-*
152 *8(rf)* shows reduced proximal arm gap junction coupling similar to *inx-8/9(0);*
153 *Ex[inx-8(DTC+, Sh-)]*, possible genetic interactions between *inx-8(rf)* and other
154 Pod mutants were explored (*Figure 1–figure supplement table 1*). Conditional
155 alleles of genes in the FAS pathway (*Figure 3A*) were used to construct double
156 mutants with *inx-8(rf)*. Alleles included: *pod-2(ye60)*, a cold-sensitive (*cs*) allele of
157 the *C. elegans* acetyl-CoA carboxylase ACC Type 1 (*Rappleye et al., 2003*); a
158 temperature-sensitive (*ts*) allele of fatty acid synthase *fasn-1(g43) (Jaramillo-*
159 *Lambert et al., 2015*); and *emb-8(hc69)*, a *ts* allele of an NADPH-cytochrome-
160 P450 reductase, likely necessary for reduction of CYP-450 enzymes involved in
161 fatty acid modifications (*Rappleye et al., 2003; Benenati et al., 2009*). Possible
162 interaction between *pod-2(ye60cs)* and *inx-8(rf)* was difficult to assess–*ye60cs*

163 grown at 15°C was quite sensitive to brief handling at room temperature. At a
164 partially restrictive temperature (22°C), *fasn-1(g43ts); inx-8(rf)* and *emb-*
165 *8(hc69ts); inx-8(rf)* double mutants exhibited markedly reduced brood sizes.
166 Similar reductions in brood size were also apparent in *emb-8(hc69ts); +/inx-8(rf)*,
167 suggesting *emb-8(hc69ts)* might be highly dose-sensitive to *inx-8(+)* levels
168 (*Figure 1–figure supplement table 1*).
169
170 **FAS pathway shifts from soma to germline after *pod-2***
171 Genetic interactions between *inx-8* and FAS genes could represent activity in the
172 same or parallel pathways. If gap junctions are positioned in the FAS pathway, it
173 might be possible to find a step within this pathway where gene function shifts
174 from a somatic to a germline focus. *C. elegans* is particularly amenable to such
175 an investigation because simple (highly repetitive) extrachromosomal arrays
176 used to rescue gene function tend to express well in the soma, whereas arrays
177 with more sequence complexity are generally required to prevent silencing of
178 multi-copy gene expression in the germline (*Kelly et al., 1997*).
179 Previous characterization of *pod-2* implied rescue by a simple array
180 (*Rappleye et al., 2003*); we likewise found that *pod-2(ye60cs)* is rescued by
181 simple extrachromosomal arrays at 15°C (see Materials and methods). In
182 contrast, 2 fosmids encoding *emb-8*, used individually to generate simple arrays,
183 yielded 65 transformed lines, only one of which rescued *emb-8(hc69ts)* at 25°C;
184 the array in this line was eventually silenced. For *fasn-1*, two fosmids used to

185 generate 93 simple array lines and 20 complex array lines failed to rescue *fasn-*
186 *1(g43ts)*. These results were consistent with a model in which FAS affecting
187 embryonic development requires *pod-2* in the soma, but shifts to a germline
188 requirement for *fasn-1* and *emb-8*.

189 To avoid misrepresentation of rescue results due to the special nature of a
190 conditional allele, null alleles of *pod-2(tn1691)* and *fasn-1(tn1762)*–simplified to
191 *(0)*–were generated using CRISPR-Cas9 methodology (*Figure 3B, C*) (Arribere *et*
192 *al*., 2014). *pod-2(0*) embryos from *pod-2(0)/+* parents arrest late in
193 embryogenesis (pretzel stage; *Figure 3D*); most *fasn-1(0)* embryos from *fasn-*
194 *1(0)/+* parents shows signs of differentiation, and many arrest late in
195 embryogenesis; occasional hatchlings emerge with probable hypodermal defects
196 (*Figure 3E-G*). *pod-2(0)* was rescued by simple extrachromosomal arrays,
197 supporting probable somatic function. Using a PCR-amplified genomic fragment
198 we were able to rescue somatic but not germline function of *fasn-1(0)* with a
199 simple or complex array (see Materials and methods). A genetically-balanced line
200 with a complex array, *hT2/ fasn-1(0)*; *Ex[fasn-1(+); sur-5::gfp(+)]*, segregates
201 healthy homozygous *fasn-1(0); Ex[fasn-1(+); sur-5::gfp(+)]* adults that lay almost
202 exclusively Pod embryos (Table 1). (*sur-5::gfp* is a co-injection marker expressed
203 in somatic cell nuclei (*Yochem et al., 19*98); corresponding extrachromosomal
204 arrays can be lost mitotically to generate mosaics—see below). Gonad arms
205 appear normal, and animals lay wild-type numbers of defective embryos (Table
206 1); many of these display polarity defects (4/14 symmetric first divisions) and

207 exhibit extra nuclei in early embryos. Embryos typically arrest prior to
208 morphogenesis (see below). We conclude this *fasn-1(+)* PCR fragment rescues
209 somatic *fasn-1* function and is either silenced in the germline or lacks an element
210 necessary for germline expression; in either case a germline requirement is
211 indicated. In sum, rescue results are consistent with a fertility requirement for
212 *pod-2* in the somatic gonad and *fasn-1* in the germline. This conclusion is
213 supported by genetic mosaic and gene expression data described below. If *inx-8*
214 gap junctions act in this pathway, it would position these junctions between *pod-2*
215 and *fasn-1* as possible mediators of mal-CoA transfer from soma to germline.
216

217 **GFP::POD-2 and GFP::FASN-1 are tissue restricted**

218 Endogenous, homozygous-viable, fertile GFP-labeled alleles of *pod-2* and *fasn-1*
219 were generated to determine if patterns of localization are consistent with
220 predicted foci of action. The GFP moiety in *gfp::pod-2(tn1765)* is expected to
221 label all 3 predicted isoforms (*Figure 3B*) (*WormBase*). GFP::POD-2 expression
222 is strongest in the intestine, and prominent in the hypodermis, gonadal sheath
223 (especially proximal sheath), CAN neuron, and excretory duct (*Figure 4A-C*).
224 *gfp::fasn-1(tn1782)* labeled at the amino terminus (*Figure 3C*) is
225 expressed in the hypodermis, gonad sheath (esp. proximal) and excretory duct;
226 intestinal and CAN neuron expression are not evident (*Figure 5A-C*). This
227 expression pattern partially overlaps with that of a *fasn-1* promoter::GFP reporter
228 fusion, which was expressed in the intestine (*Lee et al., 2010*). WormBase

229 predicts a single FASN-1 isoform, but a second in-frame ATG lies in Exon 2;
230 intestinal FASN-1 could be derived from translational initiation at this site, which
231 would not be revealed in our construct. Attempts to GFP-label FASN-1
232 downstream of this second ATG, or at the C-terminus, were unsuccessful.
233 Neither *gfp::pod-2* nor *gfp::fasn-1* is expressed in the DTC.
234 Germline expression for either GFP-tagged gene was not detected (*Figure*
235 *4C; Figure 5B*). Anti-GFP staining of dissected gonads failed to detect germline
236 GFP::POD-2 expression (*Figure 4C*). The earliest detectable GFP::FASN-1 in
237 embryos appears in developing hypodermis (*Figure 5D*); GFP::POD-2 is
238 prominent in developing hypodermis and intestine (*Figure 4D, E*). GFP::POD-2
239 expression decreases in response to starvation (*Figure 4F*).
240 Expression of both genes is consistent with primarily somatic functions.
241 Germline *fasn-1* activity may derive from low levels of maternal expression,
242 though its presence is confirmed by the late arrest phenotype of *fasn-1(0)*
243 embryos derived from *+/fasn-1(0)* parents (*Figure 3E-G*).
244
245 **INX-8 channels influence effects of overexpressed malonyl-CoA on**
246 **downstream FAS mutations**
247 If *inx-8* is required for transit of mal-CoA from soma to germline through gap
248 junctions, the fertility of mutants downstream of *pod-2* in the FAS pathway could
249 be compromised by inclusion of INX-8(T239I D24N) into somatic hemichannels.
250 Expression of an *Ex[pod-2(+); sur-5::gfp]* simple array increases the brood size of

251 *emb-8(hc69ts)* at 22°C. This increase is dependent on INX-8 hemichannel
252 integrity—*inx-8(+)* homozygotes facilitate the increase more effectively than
253 *+/inx-8(rf)* heterozygotes (*Figure 6A*). Importantly, anti-INX-8 and anti-INX-22 co-
254 localization in *emb-8(hc69ts); +/inx-8(rf)* dissected gonads is indistinguishable
255 from wild type, implying that cell adhesion is not affected (*Figure 2E*).
256 In contrast to *emb-8(hc69ts)*, expression of *Ex[pod-2(+); sur-5::gfp]* in
257 *fasn-1(g43ts)* significantly reduced brood size ($p<0.01$), and brood size reduction
258 is more severe in homozygous *inx-8(+)* than heterozygous *+/inx-8(rf)*
259 backgrounds ($p<0.05$) (*Figure 6B*). This result likely relates to the mechanism of
260 FASN production of fatty acids—acetyl-CoA (FA chain initiation) and mal-CoA
261 (chain elongation) load at a common, non-selective acyl-CoA binding site and are
262 regarded as competitive inhibitors (*Cox and Hammes, 1983; Chang and*
263 *Hammes, 1990*). Increasing the ratio of mal-CoA to acetyl-CoA may inhibit
264 FASN-1 enzyme by interfering with chain initiation. Both wild-type and enhanced
265 levels of mal-CoA delivered through wild-type INX-8 hemichannels appear to
266 inhibit *fasn-1(g43ts)*; this mutant form of FASN may be especially sensitive to
267 inhibition by higher levels of mal-CoA. Importantly, heterozygous *+/inx-8(rf)*
268 channels ameliorate this inhibition, likely by reducing mal-CoA transfer.
269 Enhancement by *inx-8(+)* hemichannels of both a positive *(emb-8)* and a
270 negative *(fasn-1)* effect on FAS mutations downstream of overexpressed *pod-*
271 *2(+)* strongly argues that *inx-8* acts in the same pathway as *pod-2*, and is

272 consistent with gap junctions acting as conveyors of mal-CoA from soma to
273 germline (*Figure 6C*).
274
275 **Genetic mosaic analyses associate *pod-2* sheath cell loss with the Pod**
276 **phenotype**
277 To verify a somatic *pod-2* focus of action, genetic mosaic animals derived from
278 *pod-2(0); Ex[pod-2(+); sur-5::gfp]* were sought. 17/833 adult hermaphrodites
279 were identified that produced dead eggs but no viable progeny; these adults were
280 examined for cell lineage loss of *Ex[pod-2(+); sur-5::gfp]*. Animals fell into two
281 classes: (1) eight animals lost *Ex[pod-2(+); sur-5::gfp]* from most or all gonad
282 sheath cells, and (2) nine animals lost *Ex[pod-2(+); sur-5::gfp]* from the intestine
283 (*Figure 7A*).
284 Within the first class of mosaics, five animals lost the array in all sheath
285 cells in both gonad arms. Three other animals exhibited a difference in
286 phenotypic severity between gonad arms—embryos derived from one arm
287 developed to later multicellular stages *in utero* (*Figure 7B-D*). Differences were
288 coincident with loss of the array from all sheath cells in the more severely
289 affected arm, versus retention of the array in a single sheath cell of the better
290 arm. In subsequent screening, five more mosaics were identified that displayed
291 phenotypic disparity between the two gonad arms; in one example, one arm
292 produced defective embryos while the better arm gave rise to wild-type embryos
293 (producing ≥40 viable progeny). These results indicate that the focus of *pod-2(0)*

294 rescue is autonomous to each gonad arm, consistent with the interpretation that
295 *pod-2* expression in the somatic sheath is essential to embryonic viability.
296 In subsequent screening for germline (P_4 –) mosaics, four animals were
297 identified that maintained the array in the soma but lost the array in all embryos
298 (*Figure 7A*). The terminal stages of embryonic development resembled those of
299 *pod-2(0)* embryos derived from *+/pod-2(0)* parents, i.e. embryos developed to 3-
300 fold or pretzel stages but failed to hatch (*Figure 7E-G*). These stages are more
301 advanced than terminal stages of many dead embryos derived from parents with
302 somatic (but not germline) loss of the rescuing array; such embryos fail to
303 differentiate (*Figure 7H*). This early developmental arrest resembles terminal-
304 stage Pod embryos from *fasn-1(0); Ex[fasn-1(+))*] (compare panels H and I in
305 *Figure 7*). We conclude that somatic *pod-2(+)* supplies sufficient levels of mal-
306 CoA to the germline not only to establish a wild-type 1-cell embryo, but also to
307 support continued development, presumably until zygotic *pod-2* expression
308 becomes adequate for completion of embryogenesis. These studies establish
309 that metabolites essential for embryonic development can be produced in the
310 somatic gonad and provided to the oocyte through gap junctions.
311
312 **Intestinal loss of *pod-2*, but not *fasn-1*, results in a germline starvation**
313 **response**
314 The other class of *pod-2(0)* genetic mosaics producing dead eggs in our original
315 screen lost *Ex[pod-2(+); sur-5::gfp]* from the intestine (E–) (*Figure 7A*). E(–)

316 mosaic animals were smaller than wild type, and gonad arms were severely
317 reduced in size (*Figure 8A*). Only the most proximal oocytes showed appreciable
318 growth. E(–) mosaic gonad arms resemble those seen in gonads undergoing the
319 oocyte starvation response, or adult reproductive diapause (ARD), a process
320 induced by starvation during the L4 larval stage proposed to maintain germline
321 stem cells for repopulation of the gonad upon the resumption of feeding (*Angelo*
322 *and Van Gilst, 2009; Seidel and Kimble, 2011*). During ARD, germline stem cells
323 cease dividing, the gonad shrinks due to extensive apoptosis of differentiated
324 germ cells, and growth is largely restricted to the most proximal oocyte.
325 The *C. elegans* intestine is rich with lipid droplets and the source of yolk,
326 and regarded as a major site of FAS (*Watts and Ristow, 2017*). A genetic
327 pathway in *C. elegans* required for intestinal apical polarity establishment leading
328 to proper lumen formation has been described; genes in this pathway, including
329 *pod-2*, encode enzymes required for glycosphingolipid synthesis (*Zhang et al.,*
330 *2012*). Lipid biosynthesis is required throughout larval growth, coincident with
331 membrane expansion. The identification of adult mosaics lacking *pod-2(+)* in the
332 intestine was therefore surprising. We subsequently identified two presumptive
333 P_1(–) *pod-2* mosaics, predicted to have lost *pod-2(+)* function in the intestine,
334 somatic gonad, germline, many muscle and hypodermal cells, among others
335 (*Figure 7A*). The most striking phenotype distinguishing these animals from E(–)
336 mosaics was an extremely constipated intestine (*Figure 8B*). The absence of this
337 constipation in E(–) mosaic animals implies that loss of *pod-2(+)* from the

338 intestine does not prevent the processing of bacteria through the intestinal lumen.
339 (Both P_1 mosaics showed tissue extruded from the rectum, which may be the
340 cause of constipation.)

341 Although *gfp::fasn-1(tn1782)* is not detected in the intestine, we asked if
342 there is a functional role for *fasn-1* similar to *pod-2*. As described above,
343 homozygous *fasn-1(0); Ex[fasn-1(+); sur-5::gfp]* progeny from heterozygous
344 parents produce Pod embryos but exhibit no other phenotype; within this class of
345 progeny we screened for E(–) mosaics. Ten (of 800) such animals were identified
346 (*Figure 7A*); in stark contrast to *pod-2*, their gonad arms appeared normal. These
347 animals displayed no overt defects outside of Pod embryo production (*Figure*
348 *8C*). Because maternal FASN-1 rescues *fasn-1(0)* homozygotes to later
349 embryonic stages, an early intestinal function for *fasn-1* equivalent to *pod-2* could
350 be rescued maternally. However, the surprising conclusion from this mosaic
351 analysis is that there is no significant intestinal requirement for zygotic *fasn-1* in
352 larval and adult stages. The implication is that the primary function of mal-CoA
353 produced in the intestine is not as substrate for intestinal FASN-1.
354

355 **Is malonyl-CoA required in other germline processes?**

356 *inx-8(rf)* and *inx-8/9(0); Ex[inx-8(DTC+, Sh-)]* share delayed oogenesis and a
357 reduction in gap junction coupling, germ cell proliferation, and brood size. *inx-*
358 *21(0)* mutants are sterile, and *inx-22(0)* mutants are fertile (*Starich et al., 2014*);
359 therefore mal-CoA required for embryos must transit through gap junction

360 channels comprised of INX-14/INX-21 hemichannels, which are expressed
361 throughout the distal arm (*Figure 2B*). We asked if mal-CoA levels might
362 influence phenotypes preceding embryogenesis, such as oocyte production.
363 Supplying mal-CoA transiently by microinjection (0.5-10 mM) into *inx-*
364 *8/9(0); Ex[inx-8(DTC+, Sh-)]* L4 gonad arms failed to ameliorate phenotypes such
365 as Pod-embryo production or low brood size. Ectopic expression of GFP::POD-2
366 in the germline in *inx-8/9(0); Ex[inx-8(DTC+, Sh-)]* or *inx-8(rf)* genetic
367 backgrounds also failed to improve phenotypes, including delayed
368 gametogenesis (*Figure 7–figure supplement 1*). However, whether endogenous
369 mal-CoA levels are altered under these conditions is uncertain.
370 Effects of global mal-CoA levels were indirectly examined by comparing
371 higher or lower *pod-2(+)* copy number rescue of *pod-2(0)*; numbers of dead eggs
372 and larvae were summed to reflect total embryo output (Table 1). Lower copy
373 number rescue coincided with reduced embryo output (84% of wild-type) and
374 lower proportion of viable larvae within a brood (~37% of total embryos) (Table
375 1). Embryo output may therefore by impacted by *pod-2* expression; however,
376 somatic cells outside the gonad could be responsible. We therefore asked
377 specifically if FAS is required within the germline. Somatically-rescued *fasn-1(0);*
378 *Ex[fasn-1(+); sur-5::gfp]* embryo output is comparable to wild-type (94%);
379 however, embryo output in the double mutant *fasn-1(0); inx-8(rf); Ex[fasn-1(+);*
380 *sur-5::gfp]* is only ~50% of *inx-8(rf)* alone (Table 1). The FAS pathway may
381 therefore play a germline role affecting embryo output. Surprisingly, *inx-8(rf)*

382 partially suppresses the embryonic lethality of *fasn-1(0); Ex[fasn-1(+); sur-5::gfp]*
383 (Table 1). Possibly the smaller gonad arms of *inx-8(rf)* may concentrate levels of
384 FASN-1 or mal-CoA. Alternatively, *Ex[fasn-1(+); sur-5::gfp]* germline expression
385 may be de-silenced in this genetic background. Further study is needed to
386 address the nature of this suppression.

387 **Discussion**

388 The genetic analysis of mutant *inx-8* soma-germline gap junction channels has
389 led us to three conclusions that have significance beyond the *C. elegans* model
390 system: (1) Mal-CoA produced in the somatic sheath is delivered through gap
391 junctions to the germline; this mal-CoA is necessary to establish a proper one-
392 cell embryo and to support continued embryogenesis. To our knowledge, this
393 segregation of the cellular source of mal-CoA from the eventual cell type in which
394 it is used as substrate is novel. As the rate-limiting step in FAS, mal-CoA
395 production is an attractive control point to tie aspects of germ cell developmental
396 progression to somatic control. (2) *pod-2* expression (and presumably mal-CoA
397 production) is exceptionally robust in the intestine and essential for normal
398 germline development. In the absence of intestinal POD-2, the germline exhibits
399 phenotypic hallmarks of germline ARD despite the presence of a replete food
400 source. By contrast, intestinal *fasn-1* expression is not similarly required. (A
401 possible caveat is that maternal *fasn-1* in the intestine may be sufficient to reach
402 adulthood, which would be surprising.) In light of the abundant expression level of
403 *gfp::pod-2* in the intestine, and our finding that mal-CoA can be directionally
404 transferred intercellularly, the question arises as to whether the intestine provides
405 mal-CoA to other cells. Alternatively, a deficit of mal-CoA production in the
406 intestine might initiate a systemic starvation response. Recently, *Gerisch et al.,*
407 (2020) have shown that the HLH-30/TEFB transcription factor functions as a
408 master regulator of the ARD state. *hlh-30* mutants fail to effect the system-wide

409 changes promoting long-term survival and recovery associated with ARD. ARD
410 longevity does not appear to rely on fatty acid metabolism. However, entry of *hlh-*
411 *30* mutants into the ARD state appears normal; therefore effects of decreased
412 mal-CoA expression in the intestine may lie upstream of *hlh-30* activity. (3) A
413 pronounced delay in gametogenesis along with reduction in brood size results
414 from reduced soma-germline gap junction communication; it is unknown if this
415 delay derives from generally slower mitotic or meiotic progression, or from a
416 developmental block at a particular meiotic stage. The nature of potential
417 molecules passing through gap junctions that are responsible for timely meiotic
418 progression is unknown, but mal-CoA has thus far not been implicated.

419 Our results are consistent with other findings in *C. elegans* related to fatty
420 acid metabolism in oocytes. *pod-2*/ACC requires post-translational covalent
421 attachment of biotin for enzymatic activity, and *bpl-1* (*b*iotin *p*rotein *l*igase-1) is
422 the *C. elegans* ortholog of the necessary holocarboxylase synthetase (*Watts et*
423 *al., 2018*). Mal-CoA provided in the bacterial diet enables *bpl-1* mutants to
424 develop to adulthood, but *de novo* synthesis of polyunsaturated fatty acids
425 (PUFAs) is required for embryonic viability (*Watts et al., 2018*). Our results
426 indicate that mal-CoA supplied for PUFA synthesis (and other FAS) in the early
427 embryo is derived from the somatic sheath via gap junctions. PUFA-dependent
428 prostaglandin signaling from oocytes influences sperm guidance, and reduction
429 of *inx-14* function disrupts this signaling (*Kubagawa et al., 2006; Edmonds et al.,*
430 *2011*). We suggest that reduced levels of mal-CoA delivered to the oocyte

431 through mutant INX-14-containing gap junctions may reduce prostaglandin
432 synthesis and its signaling function for sperm migration.

433 At least one route outside of gap junctions may deliver mal-CoA to the
434 germline early in its development. The primordial germ cells Z2 and Z3 associate
435 with a pair of intestinal cells during embryogenesis; contacts are lost before
436 hatching (*Sulston et al., 1983; Abdu et al., 2016*). Therefore an early germline
437 requirement for mal-CoA could be fulfilled directly from the intestine. Loss of such
438 a function would be encompassed within the ARD-like phenotype seen in *pod-2*
439 E(–) mosaics.

440 In addition to its metabolic function in FAS, mal-CoA has established roles
441 as a regulatory molecule. It inhibits beta-oxidation of fatty acids by mitochondria.
442 Inhibitory mal-CoA derives from a second acetyl-CoA carboxylase (ACC2),
443 associated with the mitochondrial membrane. Manipulation of mal-CoA levels in
444 the mouse hypothalamus regulates food intake (Wolfgang and Lane, 2006).
445 Regulation is effected through the brain-specific CPT1-c, via a mechanism
446 distinct from the enzymatic activity of other CPT1 enzymes (*Sierra et al., 2008;*
447 *Reilly and Mak, 2012*). Little information regarding the *C. elegans* ACC2 is
448 known; somatically-delivered mal-CoA could potentially influence germline
449 mitochondrial function.

450 Malonylation as a post-translational lysine modification has recently been
451 described (*Peng et al., 2011*). Malonylation may inhibit target proteins, such as
452 the glyocolytic enzymes glyceraldehyde 3-phosphate dehydrogenase and

453 pyruvate kinase (*Kulkarni et al., 2017*). Malonylation of mTOR reduces mTORC1
454 complex activity, decreasing endothelial cell proliferation and reducing
455 angiogenesis in a human umbilical model (*Bruning et al., 2018*). Together these
456 studies and others suggest a potentially pervasive role for mal-CoA in sensing
457 and responding to nutritional status. One trait associated with rapid tumor growth
458 is an increase in FAS, and FASN has been explored as a cancer therapy target
459 (*Menendez et al., 2007*). Possibly the ability of mal-CoA to transit through gap
460 junctions might sustain FAS during tumor progression. The discovery that mal-
461 CoA transits through gap junctions from soma to germline may be indicative of
462 other unappreciated intercellular roles for this important molecule.

463 **Materials and methods**

464 **Strains**

465 *C. elegans* strains were grown on standard NGM media (plus Nystatin, 6.25 mg/l)
466 with *E. coli* strain OP50 as food source. Temperatures used for conditional
467 mutants are indicated in main text. In addition to the wild-type strain N2, the
468 following alleles were used: Chr. *I*: *fasn-1(g43ts); fasn-1(tn1762null); fasn-*
469 *1(tn1782[gfp::fasn-1]); lin-41(tn1541[gfp::tev::s-tag::lin-41]);* Chr. *II*: *pod-*
470 *2(ye60cs); pod-2(tn1691null); pod-2(tn1765[gfp::tev::3xFLAG::pod-2]);* Chr. *III*:
471 *emb-8(hc69ts); dpy-17(e1295);* Chr. *IV*: *inx-8(tn1474null) inx-9(ok1502null); inx-*
472 *8(tn1513) inx-9(ok1502); inx-8(tn1513 tn1555) inx-9(ok1502)*—a.k.a. *inx-8(rf)* in
473 main text. Balancers used included: *tmC18 [dpy-5(tmIs1236)] I; hT2[bli-4(e937)*
474 *let-?(q782) qIs48] (I:III); mIs11 IV.* Extrachromosomal arrays used included:
475 *tnEx195[inx-8(+) inx-9(+); sur-5::gfp]; tnEx205[lag-2p::inx-8::gfp; str-1::gfp];*
476 *tnEx212[W09B6-pod-2(+)—20 ng/µl—hi copy; sur-5::gfp]; tnEx218[fasn-1(+);*
477 *sur-5::gfp]; tnEx219[W09B6-pod-2(+)—4 ng/µl—lo copy; sur-5::gfp];* and
478 *tnEx221[inx-8(tn1513 tn1555); str-1::gfp].*

479

480 **Microinjection rescue of FAS mutants with extrachromosomal arrays**

481 The cosmid W09B6 was used at 50 ng/µl (2 lines) or 20 ng/µl (1 line) with *sur-*
482 *5::gfp* (75 ng/µl) to rescue *pod-2(ye60cs). sur-5::gfp* expression was faint for both
483 lines obtained with 50 ng/µl and these were not further characterized. *pod-*
484 *2(tn1691null)* was rescued by microinjection using W09B6 at 4 ng/µl (5 lines) or

485 by crossing in *tnEx212*. Fosmids WRM0613bD07(10 ng/µl, or 50 ng/µl—1 line
486 that silenced) and WRM067cB03 (25 ng/ul) were used to attempt rescue of *emb-*
487 *8(hc69ts)*. Numerous conditions using fosmids WRM0612bD08 and
488 WRM0614aH05 in simple or complex arrays were used to try to rescue *fasn-*
489 *1(g43ts)* without success. However, FASN enzyme functions as a dimer;
490 formation of dimers between mutant (*g43*) and wild-type monomers might inhibit
491 phenotypic rescue. After *fasn-1(tn1762null)* was generated, somatic but not
492 germline rescue was obtained using a *fasn-1* genomic PCR product forming
493 simple arrays (1 ng/µl + *sur-5::gfp-75* ng/µl, at least 2/6 lines segregated *fasn-*
494 *1(0); Ex[fasn-1(+); sur-5::gfp(+)]* animals that laid only Pod embryos), or a
495 complex array (1 ng/µl + 20 ng/µl *sur-5::gfp* + 100 ng/µl salmon sperm,1 line
496 from 30 injected animals) as described in the main text.
497
498 **Recombinant DNA constructs for isolation of new *pod-2* and *fasn-1* alleles**
499 Standard CRISPR/Cas-9 methods were used to generate deletions and GFP
500 insertions in *pod-2* and *fasn-1.* For deletions, 100-nt repair templates were
501 synthesized (Ultramers; Integrated DNA Technologies, Coralville, IA, USA) and used
502 in a *dpy-10(cn64)* co-conversion strategy previously described (*Arribere et al., 2014*).
503 Injection mixes included: pDD162 (Cas9), 50 ng/µl; 25 ng/µl (*pod-2*) or 10 ng/µl (*fasn-*
504 *1*) each single guide; Ultramer repair template, 500 nM; *dpy-10* single guide (pJA58),
505 25 ng/µl; *dpy-10(cn64)* Ultramer A2-2F-827, 500nM. Single guides were made by
506 annealing oligo pairs and cloning into pRB1017 *(Arribere et al., 2014*): Deletions were

507 verified by PCR. The PCR fragment used to rescue *fasn-1(tn1762null)* was amplified
508 from genomic DNA using primers 5'-tacgtcaaacatccgtttgtcaacgtcac-3' and 5'-
509 ttcttctcctcgtcctttgatacgaagatc-3'.

510 Generation of GFP insertions into *pod-2* using pDD282 followed established
511 protocols (*Dickinson et al., 2015*). Injection mix included the single guide (10 ng/µl),
512 repair template (10 ng/µl), pDD162 (50 ng/µl), and *sur-5::gfp* (80 ng/µl). The insertion
513 was verified by sequencing PCR products generated with primers positioned outside
514 the homology arms.

515 For *gfp::fasn-1*, we were unable to isolate 3' insertions using the Dickinson
516 method (*Dickinson et al., 2015*). This method relies on isolation of candidates based
517 on the Roller phenotype, and because *fasn-1* has been implicated in molting, we
518 turned to a co-conversion approach (*Arribere et al., 2014*). A repair template was
519 generated that included the GFP sequence from pDD282, and *fasn-1* homology arms
520 on either side. The injection mix contained pDD162, 50 ng/µl; *fasn-1* single guide 10
521 ng/µl; *gfp::fasn-1* repair template, 20 ng/µl; *dpy-10* single guide (pJA58), 25 ng/µl;
522 *dpy-10(cn64)* Ultramer A2-2F-827, 500nM and pCFJ190, 2.5 ng/µl. Rol candidates
523 were screened directly for GFP expression. The insertion was verified by sequencing
524 PCR fragments generated using primers placed outside of the repair template
525 sequence.

526 *mex-5p::gfp::pod-2::tbb-2-3'UTR* was constructed by Gibson assembly of
527 component PCR products representing the *mex-5* promoter, the "a" isoform of
528 *gfp::pod-2*, and the tbb-2-3'UTR to prevent germline RNA degradation.

529 **Immunofluorescence**

530 Antibody staining of dissected gonads was as previously described (*Starich et*
531 *al., 2014*). DIC and fluorescent images were acquired on a Zeiss (Thornwood,
532 NY, USA) motorized Axioplan 2 microscope with either a 40x Plan-Neofluar
533 (numerical aperture 1.3), a 63x Plan-Apochromatic (numerical aperture 1.4), or
534 100x PlanApochromatic (N.A. 1.4) objective lens using a AxioCam MRm camera
535 and AxioVision software (Zeiss).

536

537 **Genetic mosaic analysis**

To associate the somatic focus of action of *pod-2* for germline phenotypes, array losses were characterized in animals of genotype *pod-2(1691null); tnEx212[W09B6-pod-2(+)—20 ng/µl—hi copy; sur-5::gfp]* that were isolated on the basis of sterility. Subsequently, potential candidate mosaics of interest were prescreened directly at the dissecting microscope level for asymmetry in the phenotypic severity seen between anterior and posterior gonad arms, and then examined at the compound microscope level for loss of *sur-5::gfp* expression. Potential *pod-2(tn1691null); tnEx219[W09B6-pod-2(+)—4 ng/µl—lo copy; sur-5::gfp]* genetic mosaics were also prescreened in this manner. Intestinal (E–) mosaics were prescreened using low-power fluorescence SMZ18 Nikon (Melville, NY, USA) microscope with a Lumencor (Beaverton, OR, USA) SOLA Light Engine, but for *pod-2* many of these candidate mosaics were seen to express *sur-5::gfp* at very low levels, or in just a few intestinal cells, when examined at

high power. This was not an issue when isolating *fasn-1(tn1762null); tnEx218[fasn-1(+); sur-5::gfp]* E(–) mosaics.

538 **Oligonucleotides used**

539 *fasn-1(tn1762)* isolation

540 Single guide pairs:

541 5'-tcttggtatcttcccactcactga-3' plus 5'-aaactcagtgagtgggaagatacc-3', and

542 5'-cttggatgactttccttgcacga-3' plus 5'-aaactcgtgcaaggaaagtcatcc-3'.

543

544 Repair template:5'-

545 cgtatgacgtgatttttaatgtgataattactctgaaatatctcaaaacgtgcaaggaaagtcatcttcagtaacagtt

546 gaacacatcaacaggattat-3'

547

548 Verification of *tn1762*:

549 5'- ctgacaagacgacggacaactcagg-3' and 5'- ctacgtaaccgtaacggcatggcac-3'

550

551 *pod-2(tn1691)* isolation

552 Single guide pairs:

553 5'-tcttggaaaactgtccatatacaa-3' plus 5'-aaacttgtatatggacagttttcc-3', and

554 5'-tcttgacagaacaggaaaaagtgg-3' plus 5'-aaacccagtttttcctgttctgtc-3'.

555

556 Repair template: 5'-

557 ccgatttttgtgcaatttcagagcaatataagtatataaacgttattttcagagccatcacttttcctgttctgtgatata

558 caagaaacctattcagtgccttatttgattgacgactac-3'

559

560 Verification of *tn1691*employed oligos:

561 5'-cgacgaagtaagtgagcctaattgtac-3' with 5'-ttgtcaaccaccttacagtggcatg-3'

562

563 <u>*gfp::pod-2(tn1765)* isolation</u>

564 Single guide pair:

565 5'-tcttgcagggttacggatcttgga-3' and 5'-aaactccaagatccgtaaccctgc-3

566 Homology arm oligo pairs:

567 5'-acgttgtaaaacgacggccagtcgccggcatctacctgtgtacctgacctgaccagattc-3' plus

568 5'-aactccagtgaacaattcttctcctttactcattgtgaatgccagtccaagatccgtaac-3';

569 5'-cgtgattacaaggatgacgatgacaagagagttgtaaacgggcaaaaaccagatatcag-3' plus

570 5'-tcacacaggaaacagctatgatatgtgagagtgaatgaactgctccatgctctc-3'

571

572 <u>*gfp::fasn-1(tn1782)* isolation</u>

573 Single guide pair:

574 5'-tcttgaaggatcgtccgattcgag-3' plus 5'-aaaactcgaatcggacgatccttc-3'

575 Primer used to introduce silent mutations to recognition site:

576 5'-gataatactggagagggctcatcagactcaagtggaacttgggagcgaatttcggac-3'

577 Homology flanking GFP:

578 5’-gggataataagtaggttctgacctcctctcccg-3’ to 5’-gatccattcgtgcttcttcttgtcccgtgag-3’

579

Acknowledgements

We are grateful to our colleagues Gabriela Huelgas-Morales, Caroline Spike, Tatsuya Tsukamoto, and Jocelyn Shaw for discussions regarding experiments and comments on the manuscript. We would also like to thank Ross Johnson and David Hall for many years of sharing their knowledge and enthusiasm in all things concerning gap junctions. This work was supported by National Institutes of Health (NIH) grant GM57173 to DG. Some strains were provided by the Caenorhabditis Genetics Center, which is funded by grant P40OD010440 from the NIH Office of Research Infrastructure Programs.

Additional information

Funding

Funder	Grant reference number	Author
National Institutes of Health	GM57173	David Greenstein

Author contributions

TS conducted the experiments, prepared the figures, and wrote the manuscript. TS and DG designed and conceptualized the research study. DG obtained funding, supervised the study, and edited the manuscript.

580

References

Abdu Y, Maniscalco C, Heddleston, JM, Chew, T-L, Nance J. 2016. Developmentally programmed germ cell remodelling by endodermal cell cannibalism. *Nature Cell Biology* **18**:1302–1310. DOI: 10.1038/ncb3439, PMID: 27842058

Angelo G, Van Gilst MR. 2009. Starvation protects germline stem cells and extends reproductive longevity in *C. elegans*. *Science* **326**:954–958. DOI: 10.1126/science.1178343, PMID: 19713489

Arribere JA, Bell RT, Fu BX, Artiles KL, Hartman PS, Fire AZ. 2014. Efficient marker-free recovery of custom genetic modifications with CRISPR/Cas9 in *Caenorhabditis elegans*. *Genetics* 198:837–846. DOI: 10.1534/genetics.114.169730, PMID: 25161212

Austin J, Kimble J. 1987. *glp-1* is required in the germ line for regulation of the decision between mitosis and meiosis in *C. elegans*. *Cell* **51**:589–599. DOI: 10.1016/0092-8674(87)90128-0, PMID: 3677168

Austin J, Kimble J. 1988. Transcript analysis of *glp-1* and *lin-12*, homologous genes required for cell interactions during development of *C. elegans*. *Cell* **58**:565–571. DOI: 10.1016/0092-8674(89)90437-6, PMID: 2758467

Benenati G, Penkov S, Müller-Reichert T, Entchev EV, Kurzchalia TV. 2009. Two cytochrome P450s in *Caenorhabditis elegans* are essential for the organization of eggshell, correct execution of meiosis and polarization of the embryo.

Mechanisms of Development **126**:382–393. DOI: 10.1016/j.mod.2009.02.001, PMID: 19368796

Berman HM, Westbrook J, Feng Z, Gilliland G, Bhat TN, Weissig H, Shindyalov IN, Bourne PE. 2000. The protein data bank. *Nucleic Acids Research* **28**:235–242. DOI: 10.1107/s0907444902003451, PMID: 10592235

Bruning U, Morales-Rodriguez F, Kalucka J, Goveia J, Taverna F, Queiroz KCS, Dubois C, Cantelmo AR, Chen R, Loroch S, Timmerman E, Caixeta V, Bloch K, Conradi LC, Treps L, Staes A, Gevaert K, Tee A, Dewerchin M, Semenkovich CF, Impens F, Schilling B, Verdin E, Swinnen JV, Meier JL, Kulkarni RA, Sickmann A, Ghesquière B, Schoonjans L, Li X, Mazzone M, Carmeliet P. 2018. Impairment of angiogenesis by fatty acid synthase inhibition involves mTOR malonylation. *Cell Metabolism* **28**:866–880. DOI: 10.1016/j.cmet.2018.07.019, PMID: 30146486

Chang S-I, Hammes GG. 1990. Structure and mechanism of action of a multifunctional enzyme: fatty acid synthase. *Accounts of Chemical Research* **23**:363–369. DOI: https://doi.org/10.1021/ar00179a003

Cox BG, Hammes GG. 1983. Steady-state kinetic study of fatty acid synthase from chicken liver. *Proceedings of the National Academy of Sciences USA* **80**:4233–4237. DOI: 10.1073/pnas.80.14.4233, PMID: 6576333

Dickinson DJ, Pani AM, Heppert JK, Higgins CD, Goldstein B. 2015. Streamlined genome engineering with a self-excising drug selection cassette. *Genetics* **200**:1035–1049. DOI: 10.1534/genetics.115.178335, PMID: 26044593

Edmonds JW, McKinney SL, Prasain JK, Miller MA. 2011. The gap junctional protein INX-14 functions in oocyte precursors to promote *C. elegans* sperm guidance. *Developmental Biology* **359**:47–58. DOI: 10.1016/j.ydbio.2011.08.014, PMID: 21889935

Gerisch B, Tharyan RG, Mak J, Denzel SI, Popkes-van Oepen T, Henn N, Antebi A. 2020. HLH-30/TFEB is a master regulator of reproductive quiescence. *Developmental Cell* **53**:1–14. DOI: 10.1016/j.devcel.2020.03.014, PMID: 32302543

Govindan JA, Cheng H, Harris JE, Greenstein D. 2006. $G\alpha_{o/i}$ and $G\alpha_s$ signaling function in parallel with the MSP/Eph receptor to control meiotic diapause in *C. elegans*. *Current Biology* **16**:1257–1268. DOI: 10.1016/j.cub.2006.05.020, PMID: 16824915

Henderson, ST, Gao D, Lambie EJ, Kimble J. 1994. *lag-2* may encode a signaling ligand for the GLP-1 and LIN-12 receptors of *C. elegans*. *Development* **120**:2913–2924. PMID: 7607081

Jaramillo-Lambert A, Fuchsman AS, Fabritius AS, Smith HE, Golden A. 2015. Rapid and efficient identification of *Caenorhabditis elegans* legacy mutations using Hawaiian SNP-based mapping and whole-genome sequencing. *G3* **5**:1007–1019. DOI: 10.1534/g3.115.017038, PMID: 25740937

Johnston WL, Krizus A, Dennis JW. 2006. The eggshell is required for meiotic fidelity, polar-body extrusion and polarization of the *C. elegans* embryo. *BMC Biology* **4**:35. DOI: 10.1186/1741-7007-4-35, PMID: 17042944

Kelly WG, Montgomery MK, Fire A. 1997. Distinct requirements for somatic and germline expression of a generally expressed *Caenorhabditis elegans* gene. *Genetics* **146**:227–238. PMID: 9136012

Kubagawa HM, Watts JL, Corrigan C, Edmonds JW, Sztul E, Browse J, Miller MA. 2006. Oocyte signals derived from polyunsaturated fatty acids control sperm recruitment *in vivo*. *Nature Cell Biology* **8**:1143–1148. DOI: 10.1038/ncb1476, PMID: 16998478

Kulkarni RA, Worth AJ, Zengeya TT, Shrimp JH, Garlick JM, Roberts AM, Montgomery DC, Sourbier C, Gibbs BK, Mesaros C, Tsai YC, Das S, Chan KC, Zhou M, Andresson T, Weissman AM, Linehan WM, Blair IA, Snyder NW, Meier JL. 2017. Discovering targets of non-enzymatic acylation by thioester reactivity profiling. *Cell Chemical Biology* **24**:231–242. DOI: 10.1016/j.chembiol.2017.01.002, PMID: 28163016.

Lee K-Z, Kniazeva M, Han M, Pujol N, Ewbank, J. 2010. The fatty-acid synthase *fasn-1* acts upstream of WNK and Ste20/GCK-VI kinases to modulate antimicrobial peptide expression in *C. elegans* epidermis. *Virulence* **1**:113–122. DOI: 10.4161/viru.1.3.10974, PMID: 21178429

McCarter J, Bartlett B, Dang T, Schedl T. 1997. Soma-germ cell interactions in *Caenorhabditis elegans*: multiple events of hermaphrodite germline development require the somatic sheath and spermathecal lineages. *Developmental. Biology* **181**:121–143. DOI: 10.1006/dbio.1996.8429, PMID: 9013925

Menendez JA, Lupu R. 2007. Fatty acid synthase and the lipogenic phenotype in cancer pathogenesis. *Nature Reviews Cancer* **7**:763–777. DOI: 10.1038/nrc2222, PMID: 17882277

Meyer RA, Laird DW, Revel J-P, Johnson RG. 1992. Inhibition of gap junctions and adherens junction assembly by connexin and A-CAM antibodies. *Journal of Cell Biology* **119**:179–189. DOI: 10.1083/jcb.119.1.179, PMID: 1326565

Mok DZL, Sternberg PW, Inoue T. 2015. Morphologically defined sub-stages of *C. elegans* vulval development in the fourth larval stage. *BMC Developmental. Biology* **15**: 26. DOI: 0.1186/s12861-015-0076-7, PMID: 26066484

Nadarajan S, Govindan JA, McGovern M, Hubbard EJ, Greenstein D. 2009. MSP and GLP-1/Notch signaling coordinately regulate actomyosin-dependent cytoplasmic streaming and oocyte growth in *C. elegans*. *Development* **136**: 2223–2234. DOI: 10.1242/dev.034603, PMID: 19502484

Olson SK, Bishop JR, Yates JR, Oegema K, Esko JD. 2006. Identification of novel chondroitin proteoglycans in *Caenorhabditis elegans*: embryonic cell division depends on CPG-1 and CPG-2. *Journal of Cell Biology* **173**:985–994. DOI: 10.1083/jcb.200603003 PMID, 16785326

Oshima A, Tani K, Fujiyoshi Y. 2016. Atomic structure of the innexin-6 gap junction channel determined by cryo-EM. *Nature Communications* **7**:1368. DOI: 10.1038/ncomms13681, PMID: 27905396

Peng C, Lu Z, Xie Z, Cheng Z, Chen Y, Tan M, Luo H, Zhang Y, He W, Yang K, Zwaans BM, Tishkoff D, Ho L, Lombard D, He TC, Dai J, Verdin E, Ye Y, Zhao

Y. 2011. The first identification of lysine malonylation substrates and its regulatory enzyme. *Molecular and Cellular Proteomics* **10**:M111.012658. DOI: 10.1074/mcp.M111.012658, PMID: 21908771

Rappleye CA, Paredez AR, Smith CW, McDonald KL, Aroian RV. 1999. The coronin-like protein POD-1 is required for anterior-posterior axis formation and cellular architecture in the nematode *Caenorhabditis elegans*. *Genes and Development* **13**:2838–2851. DOI: 10.1101/gad.13.21.2838, PMID: 10557211

Rappleye CA, Tagawa A, Le Bot N, Ahringer J, Aroian RV. 2003. Involvement of fatty acid pathways and cortical interaction of the pronuclear complex in *Caenorhabditis elegans* polarity. *BMC Developmental Biology* **3**:8. DOI: 10.1186/1471-213X-3-8, PMID: 14527340

Rappleye CA, Tagawa A, Lyczak R, Bowerman B, Aroian RV. 2002. The anaphase-promoting complex and separin are required for embryonic anterior-posterior axis formation. *Developmental Cell* **2**:195–206. DOI: 10.1016/s1534-5807(02)00114-4, PMID: 11832245

Reilly PT, Mak TW. 2012. Molecular pathways: tumor cells co-opt the brain-specific metabolism gene *CPT1C* to promote survival. *Clinical Cancer Research* **18**:5850–5855. DOI: 10.1158/1078-0432.CCR-11-3281, PMID: 22952346

Rose AS, Bradley AR, Valasatava Y, Duarte JM, Prlic A, Rose PW. 2018. NGL viewer: web-based molecular graphics for large complexes. *Bioinformatics* 34:3755–3758. DOI: 10.1093/bioinformatics/bty419, PMID: 29850778

Seidel HS, Kimble, J. 2011. The oogenic germline starvation response in *C. elegans*. *PloS ONE* **6**:e28074. DOI: 10.1371/journal.pone.0028074, PMID: 22164230

Sierra AY, Gratacós E, Carrasco P, Clotet J, Ureña J, Serra D, Asins G, Hegardt FG, Casals N. 2008. CPT1c is localized in endoplasmic reticulum of neurons and has carnitine palmitoyltransferase activity. *Journal of Biological Chemistry* **283**:6878–6885. DOI: 10.1074/jbc.M707965200, PMID: 18192268

Skerrett IM, Williams JBA. 2017. A structural and functional comparison of gap junction channels composed of connexins and innexins. *Developmental Neurobiology* **77**:522–547. DOI: 10.1002/dneu.22447, PMID: 27582044

Spike CA, Coetzee D, Eichten C, Wang X, Hansen D, Greenstein D. 2014. The NHL-TRIM protein LIN-41 and the OMA RNA-binding proteins antagonistically control the prophase-to-metaphase transition and growth of *C. elegans* oocytes. *Genetics* **198**:1535–1558. DOI: 10.1534/genetics.114.168831, PMID: 25261698

Starich TA, Hall DH, Greenstein D. 2014. Two classes of gap junction channels mediate soma-germline interactions essential for germline proliferation and gametogenesis in *C. elegans. Genetics* **198**:1127–1153. DOI: 10.1534/genetics.114.168815, PMID: 25195067

Sulston JE, Schierenberg E, White JG, Thomson JN. 1983. The embryonic cell lineage of the nematode *Caenorhabditis elegans*. *Developmental Biology* **100**: 64–119. DOI: 10.1016/0012-1606(83)90201-4, PMID: 6684600

Tagawa A, Rappleye CA, Aroian RV. 2001. *pod-2*, along with *pod-1*, defines a new class of genes required for polarity in the early *Caenorhabditis elegans* embryo. *Developmental Biology* **233**:412–424. DOI: 10.1006/dbio.2001.0234, PMID: 11336504

Watts JS, Morton DG, Kemphues KJ, Watts JL. 2018. The biotin-ligating protein BPL-1 is critical for lipid biosynthesis and polarization of the *Caenorhabditis elegans* embryo. *Journal of Biological Chemistry* **293**:610–622. DOI: 10.1074/jbc.M117.798553, PMID: 29158261

Watts JL, Ristow M. 2017. Lipid and carbohydrate metabolism in *Caenorhabditis elegans*. *Genetics* **207**:413–446. DOI: 10.1534/genetics.117.300106, PMID: 28978773

Whitten SJ, Miller MA. 2007. The role of gap junctions in *Caenorhabditis elegans* oocyte maturation and fertilization. *Developmental Biol*ogy **301**:432–446. DOI: 10.1016/j.ydbio.2006.08.038, PMID: 16982048

Wolfgang MJ, Lane MD. 2006. The role of hypothalamic malonyl-CoA in energy homeostasis. *Journal of Biological Chemistry* **281**:37265–37269. DOI: 10.1074/jbc.R600016200, PMID: 17018521

WormBase (www.wormbase.org).

Yochem J, Gu T, Han, M. 1998. A new marker for mosaic analysis in *Caenorhabditis elegans* indicates a fusion between hyp6 and hyp7, two major components of the hypodermis. *Genetics* **149**:1323–1334. PMID: 9649523

Zhang H, Abraham N, Khan LA, Hall DH, Fleming JT, Göbel V. 2012. Apicobasal domain identities of expanding tubular membranes depend on glycosphingolipid biosynthesis. *Nature Cell Biology* **13**:1189–1201. DOI: 10.1038/ncb2328, PMID: 21926990

Zhang Y, Foster JM, Nelson LS, Ma D, Carlow, CKS. 2005. The chitin synthase genes *chs-1* and *chs-2* are essential for *C. elegans* development and responsible for chitin deposition in the eggshell and pharynx, respectively. *Developmental Biol*ogy **285**:330–339. DOI: 10.1016/j.ydbio.2005.06.037, PMID: 16098962

581 **Figure Legends**

582 **Figure 1**. Ovulation and oocyte development are delayed in *inx-8(rf).* (A)
583 Diagram of adult *C. elegans* gonad. Posterior arm shows the positions of the
584 somatic distal tip cell (DTC) and five pairs of sheath cells (nuclei are numbered).
585 Anterior arm shows the underlying germline, approximate regions of germ cell
586 proliferation (Prolif.), meiotic pachytene stage (Pach.), and developing oocytes.
587 Embryos typically undergo some cell division in the uterus before being laid. Sp,
588 spermatheca; vul, vulva. (B) Compared to wild type (N2), ovulation in *inx-*
589 *8(tn1513 tn1555rf)* mutants (a.k.a. *inx-8[rf]*) is delayed ~18 hrs. Bars
590 representing 1-3 hr windows indicate approximate time of the fourth larval stage
591 (L4 to adult) molt, followed by time of appearance of the first fertilized embryo
592 ovulated into the uterus. (C) Onset of *gfp::lin-41* expression as a marker of
593 oocyte development is delayed in *inx-8(rf)*. Panels show DIC images of vulval
594 development (left), loop region of gonad arm (middle), and expression of *gfp::lin-*
595 *41* (right). Wild-type hermaphrodites express *gfp::lin-41* by the approximate L4.7
596 sub-stage of vulval development (vul); *inx-8(rf)* hermaphrodites do not express
597 *gfp::lin-41* until after vulval development is complete but before the L4-to-adult
598 molt. Null *inx-8(tn1474) inx-9(ok1502)* hermaphrodites, rescued for *inx-8::gfp*
599 expression in the DTC with *Ex[lag-2p::inx-8::gfp]*—a.k.a. *inx-8/9(0); Ex[inx-*
600 *8(DTC+, Sh-)]*—show a similar delayed onset of *gfp::lin-41* expression as *inx-*
601 *8(rf)*. Bar, 20 µm.

602 **Figure supplement 1.** Predicted topological sites of amino acids mutated in *inx-*
603 *8(tn1513 tn1555) inx-9(0)*.

604 **Figure supplement table 1**. *inx-8(rf)* exhibits reduced brood size and interacts
605 with FA synthesis pathway genes.
606 **Figure supplement table 2**. Reduced soma-germline gap junction coupling
607 delays gametogenesis.
608
609 **Figure 2.** INX-8(T239I D24N) compromises gap junction formation between
610 soma and germline. (A) Somatic INX-8 in wild-type (WT) gonads localizes to
611 puncta representing soma-germline gap junctions where DTC or sheath cells
612 overlie germ cells. (B) In WT distal gonad arms, gap junction puncta aggregate in
613 small clusters associated with each germ cell; in *inx-8(rf)* distal arms, gap
614 junction puncta localize more apically, where sheath dips down between germ
615 cells, outlining the cell (honeycomb pattern). Localization of INX-21 and INX-22
616 define the two different classes of germline gap junction hemichannels, both of
617 which include INX-14 subunits. (C) At the loop region, WT gap junction puncta
618 form large higher-order aggregates (arrows) which are absent in *inx-8(rf)*. (D) In
619 WT proximal arms, gap junction formation with INX-22-containing hemichannels
620 is extensive; in *inx-8(rf)*, INX-22 and INX-8(T239I D24N) are strongly expressed
621 but show little evidence of gap junction formation. "–1" indicates the most
622 proximal oocyte; *inx-8(rf)* hermaphrodites frequently show undersized oocytes at
623 this position as well (<). (E) Heterozygous *+/inx-8(rf)* shows little effect on gap
624 junction localization in an *emb-8(hc69ts)* background. Antibodies specific to INX-
625 8, INX-21, or INX-22 were used as indicated. DAPI-stained DNA in blue. Bar, 50
626 µm.

627 **Figure supplement 1.** INX-8(rf)::GFP can be endocytosed by oocytes.

628

629 **Figure 3.** (A) Predicted assignment of FAS mutants in a simplified FAS pathway.
630 Targeted deletions and GFP insertions are shown for *pod-2* (B) and *fasn-1* (C).
631 Predicted isoforms for POD-2 are indicated. (D-G) Terminal phenotypes of (D)
632 *pod-2(0)* and (E-G) *fasn-1(0)* mutant embryos from heterozygous *+/(0)* parents.
633 Arrows in (D) and (F) indicate differentiated anterior pharynx; arrow in (E)
634 indicates differentiated intestinal cells that formed gut granules. Bar, 20 μm.

635

636 **Figure 4**. GFP::POD-2 expression. (A) Expression in the head includes
637 hypodermis (carets) and excretory duct cell (arrow). Int, intestine. (B) Primary
638 expression in the tail includes hypodermis (carets) and intestine (Int). Left panel
639 DIC image, right panel GFP fluorescence in live animals. (C) Dissected animal
640 stained with anti-GFP antibody shows abundant intestinal expression (Int) and
641 strong expression in proximal sheath of exposed gonad arm (prox) that
642 diminishes in the distal arm. No germline expression is seen in the distal arm
643 where germ cells are revealed due to the absence of sheath coverage. Arrow
644 indicates CAN neuron, one of the few neurons essential for viability in *C.*
645 *elegans*. DAPI-staining of DNA in blue. (D, E) Earliest expression in embryos is
646 evident in developing hypodermis and intestine. (A, B, D, E) DIC images in left
647 panels, live GFP fluorescence in right panels. Bars, 20 μm, except (C) 200 μm.
648 (F) GFP::POD-2 is responsive to starvation. Top row, animals briefly washed and

649 transferred to bacteria-free NGM plates for 4 hours; lower row, animals similarly-
650 treated but fed.
651
652 **Figure 5**. GFP::FASN-1 expression. (A) GFP::FASN-1 is expressed throughout
653 the hypodermis (small arrows). Excretory duct cell expression is also indicated
654 (larger arrow). (B) Arrow indicates proximal gonad sheath expression. (C) Arrow
655 indicates developing vulva. (D) Earliest expression in developing embryos is
656 seen in hypodermis. DIC images in upper panels, live GFP fluorescence in lower
657 panels. Bars, 20 μm.
658
659 **Figure 6.** Wild-type INX-8 facilitates effects of *Ex[pod-2(+)]* overexpression on
660 conditional mutations downstream in the fatty acid synthesis (FAS) pathway.
661 Brood size was measured as the number of viable progeny produced. The
662 balancer *mIs11* provided *inx-8(+)* for all strains listed. (A) Embryonic lethality in
663 *emb-8(ts)* mutants at 22°C is more severe in heterozygous *+/inx-8(rf)* than *inx-*
664 *8(+)* backgrounds *(1)*. Expression of *Ex[pod-2(+)]* in *emb-8(ts)* significantly
665 rescues embryonic lethality *(2)*. Rescue of *emb-8(ts)* by *Ex[pod-2(+)]* is also
666 dependent on *inx-8(+)* copy number *(3)*. (B) Expression of *Ex[pod-2(+)]* in *fasn-*
667 *1(ts)* mutants at 20°C reduces brood size *(1)*. *fasn-1(ts); inx-8(+)* homozygotes
668 show greater embryonic lethality than *fasn-1(ts); (+)/inx-8(rf*) heterozygotes in the
669 absence *(2)* or presence *(3)* of *Ex[pod-2(+)].* Averages indicated with dotted
670 lines. Probability was calculated using Student's 2-tailed *t*-test. (C) Enzymes
671 (purple) implicated in germline FAS. Malonyl-CoA transits from soma sheath to

672 germline through gap junction channels comprised of INX-8/9 (soma) and INX-
673 14/INX-21 (germline) hemichannels. Germline FASN-1 uses malonyl-CoA to
674 synthesize palmitate, which may be further extended and modified to produce
675 other long-chain fatty acids. EMB-8 (NADPH-dependent CYP450 reductase) and
676 POD-7/8 (CYP450s) are necessary to synthesize the lipid-rich (inner) layer of the
677 eggshell and support polarity establishment (*Rappleye et al., 2003; Benenati et*
678 *al., 2009*); the composition of lipid layer fatty acids is unknown. *de novo* PUFA
679 synthesis is required in the germline for embryonic viability, and is implicated in
680 sperm guidance (*Kubagawa et al., 2006; Watts et al., 2018*). The identities of
681 other long-chain fatty acids that may be synthesized in the germline are
682 unknown. PUFAs, polyunsaturated fatty acids; LFAs, long-chain fatty acids;
683 MUFA, monounsaturated fatty acids; pm, plasma membrane.
684 **Source data 1.** Viable progeny counts for the Figure 6 panels A, B.
685
686 **Figure 7.** Genetic mosaic analyses of *pod-2* reveal a mal-CoA requirement in
687 somatic gonad sheath. (A) Abbreviated cell lineage of *C. elegans*. Mosaics
688 characterized correspond to loss of *sur-5::gfp* expression in the germline (P_4),
689 intestine (E), or somatic gonad. Five *pod-2(0); Ex[pod-2(+); sur-5::gfp]* animals
690 lost the array from all somatic gonad sheath cells and produced no viable
691 embryos. (B) Eight animals showed differences in array retention in each gonad
692 arm with phenotypic consequences. Arrays were generated by microinjecting
693 cosmid W09B6 *[pod-2(+)]* at 4 ng or 20 ng/µl (low/high copy). (C) Uterus of non-
694 mosaic *pod-2(0); Ex[pod-2(+)*—high copy*]* hermaphrodite; developmental

695 progression of embryos from each gonad arm is comparable. (D) Mosaic *pod-*
696 *2(0); Ex[pod-2(+)*—high copy*]* with array lost from posterior gonad arm sheath
697 but retained in a single Sh4 cell of anterior arm. Anterior arm embryos have more
698 distinct eggshells and develop to later stages. (E-H) Embryonic development
699 depends on somatic levels of mal-CoA. Shown are terminal-stage *pod-2(0)*
700 embryos derived from parents of designated genotypes. (E) Pretzel-stage
701 embryo from *+/pod-2(0)*. (F) 3-fold stage embryo from *pod-2(0); Ex[pod-2(+)—*
702 *low copy]*, with array maintained in soma but lost in the germline (P4–). (G)
703 Pretzel-stage embryo from P4(–) mosaic *pod-2(0); Ex[pod-2(+)—high copy]*. (H)
704 Embryo from mosaic *pod-2(0); Ex[pod-2(+)—low copy]* with uncharacterized
705 somatic loss of array, but array retained in the germline (P4+). This parent
706 produced exclusively dead embryos. (I) Typical terminal undifferentiated *fasn-*
707 *1(0)* Pod embryo from *fasn-1(0); Ex[fasn-1(+)]*. ant ute, anterior uterus; post ute,
708 posterior uterus; v, vulva; –1, most proximal oocyte. Bar, 20 µm.
709 **Figure supplement 1.** Expression of *gfp::pod-2* in the germline fails to rescue
710 *inx-8(rf)* phenotypes.
711
712 **Figure 8**. Mosaic loss from the intestine of *pod-2*, but not *fasn-1,* leads to an
713 ARD-like gonad arm. (A) E(–) genetic mosaic *pod-2(0); Ex[pod-2(+); sur-5::gfp]*
714 gonad arms (from same animal). Gonad arm on right partially outlined. (B) Two
715 focal planes of a presumptive P_1(–) *pod-2(0); Ex[pod-2(+); sur-5::gfp]* mosaic with
716 constipated intestine. Upper plane (left) with partially outlined intestine; lower
717 plane (right) shows underlying distal gonad arm. int, intestine; p, pachytene

718 region; v, vulva. (C) E(–) genetic mosaic *fasn-1(0); Ex[fasn-1(+); sur-5::gfp]*

719 gonad arm. –1, most proximal oocyte. Bars, 20 μm.

Table 1

Brood sizes suggest FA synthesis influences embryo output

Genotype	Larvae	Dead embryos	Total (embryo output)
Wild type (N2)	291±29 (n=33)	2±2	293±29
inx-8(rf)	108±40 (n=90)	11±6 (n=30)	119±42
inx-8/9(0); Ex[inx-8(DTC+,Sh-)]	2±2 (n=32)	19±13	20±14
pod-2(0); Ex[pod-2(+)] high copy (20 ng/µl)	164±50 (n=31)	118±41	282±59
pod-2(0); Ex[pod-2(+)] low copy (4 ng/µl)	91±24 (n=41)	156±37	247±50
fasn-1(0); Ex[fasn-1(+)	0.05 (n=80)	276±18 (n=16)	276±18
fasn-1(0); inx-8(rf); Ex[fasn-1(+)]	17±15 (n=47)	43±27	60±37

Source data 1. Brood counts for genotypes shown in Table 1.

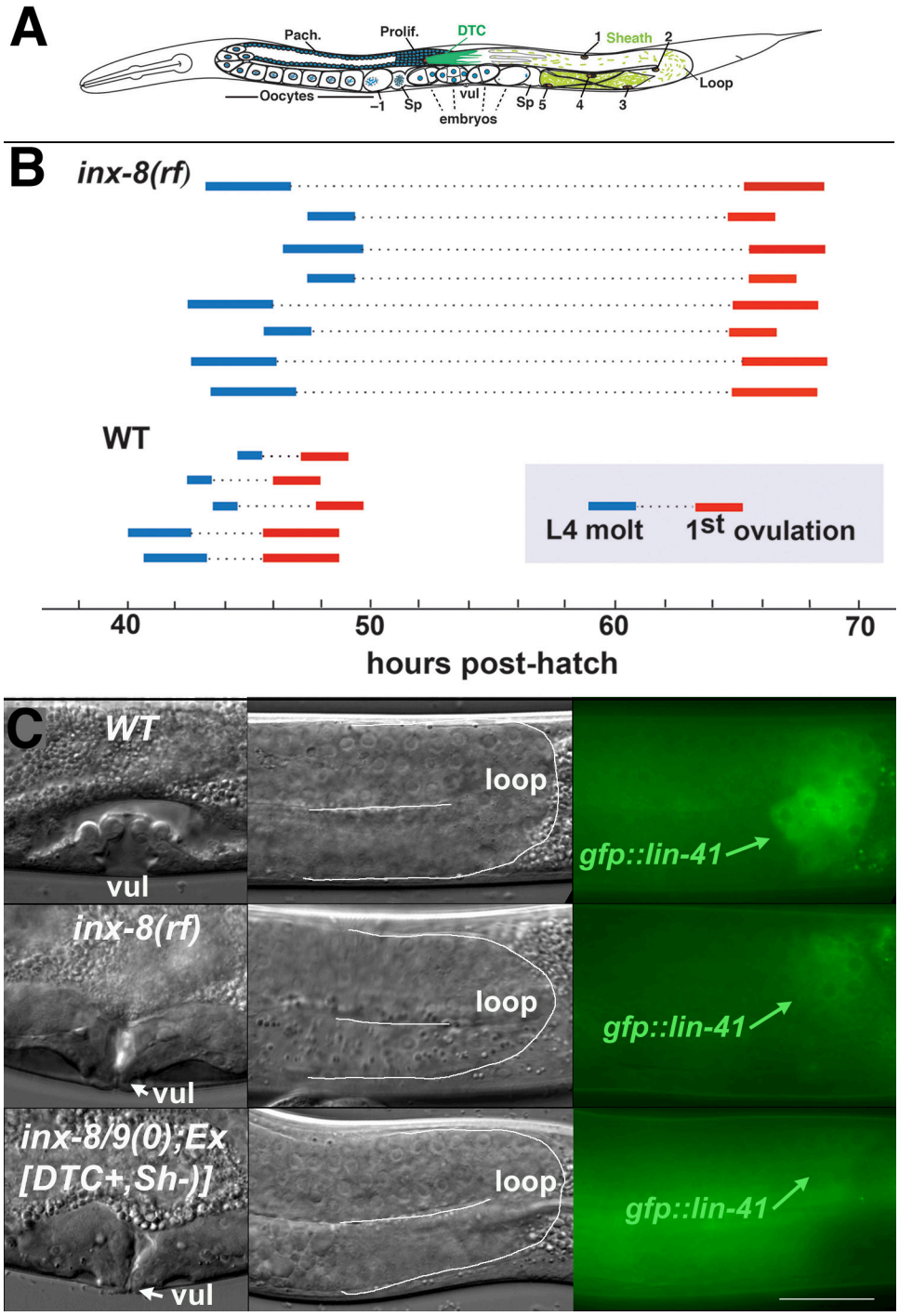
A
Pach.
Prolif.
DTC
1 Sheath 2
Loop
Oocytes
–1
Sp
vul
embryos
Sp 5
4
3
B
inx-8(rf)
WT
L4 molt
1st ovulation
40
50
60
70
hours post-hatch
C
WT
vul
loop
gfp::lin-41
inx-8(rf)
vul
loop
gfp::lin-41
inx-8/9(0);Ex
[DTC+,Sh-)]
vul
loop
gfp::lin-41

Figure 1

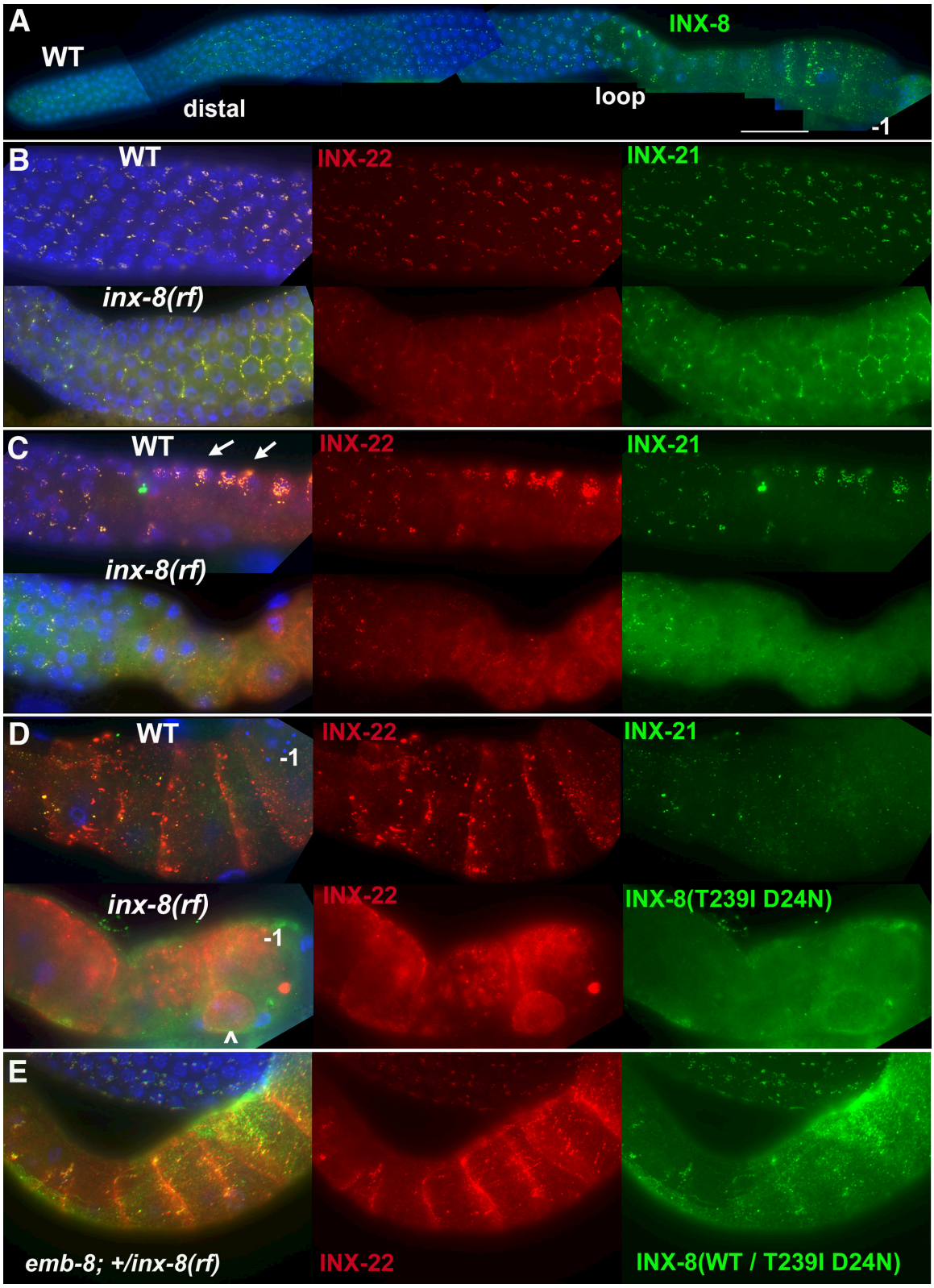
A
WT
INX-8
distal
loop
-1
B
WT
INX-22
INX-21
inx-8(rf)
C
WT
INX-22
INX-21
inx-8(rf)
D
WT
-1
INX-22
INX-21
inx-8(rf)
-1
INX-22
INX-8(T239I D24N)
E
emb-8; +/inx-8(rf)
INX-22
INX-8(WT / T239I D24N)

Figure 2

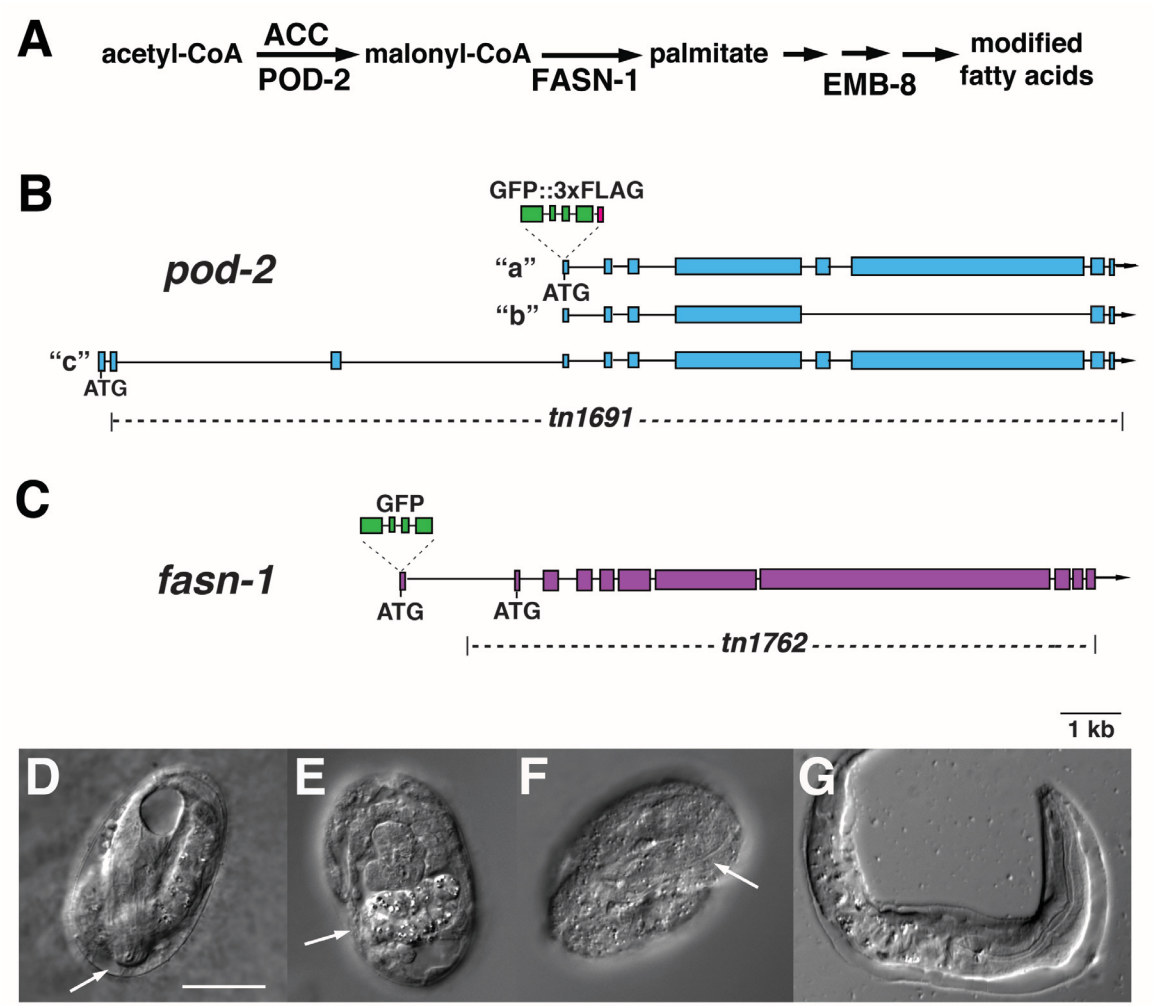
A
acetyl-CoA
ACC
POD-2
malonyl-CoA
FASN-1
palmitate
EMB-8
modified
fatty acids
B
GFP::3xFLAG
pod-2
"a"
ATG
"b"
"c"
ATG
tn1691
C
GFP
fasn-1
ATG
ATG
tn1762
1 kb
D
E
F
G

Figure 3

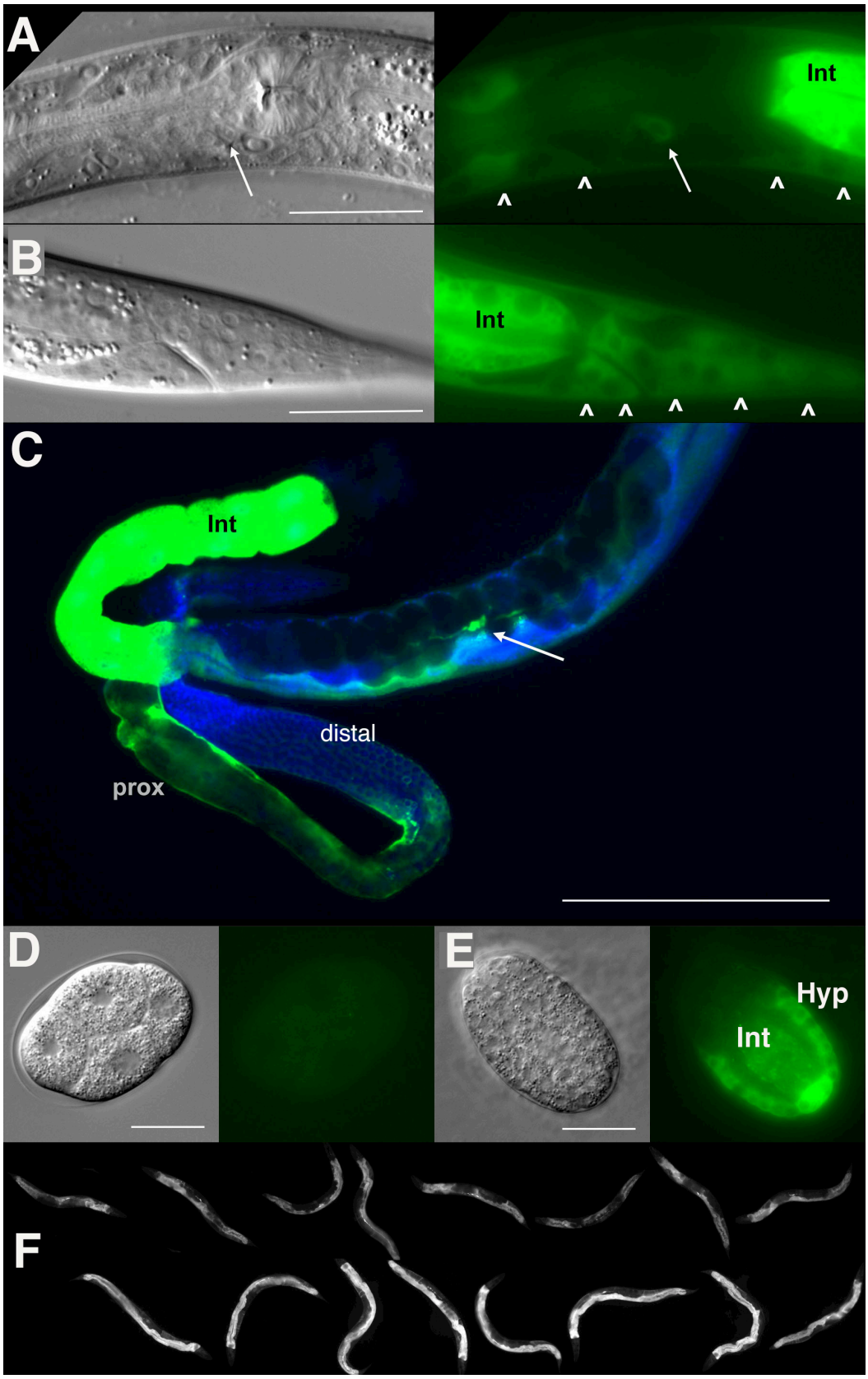

Figure 4

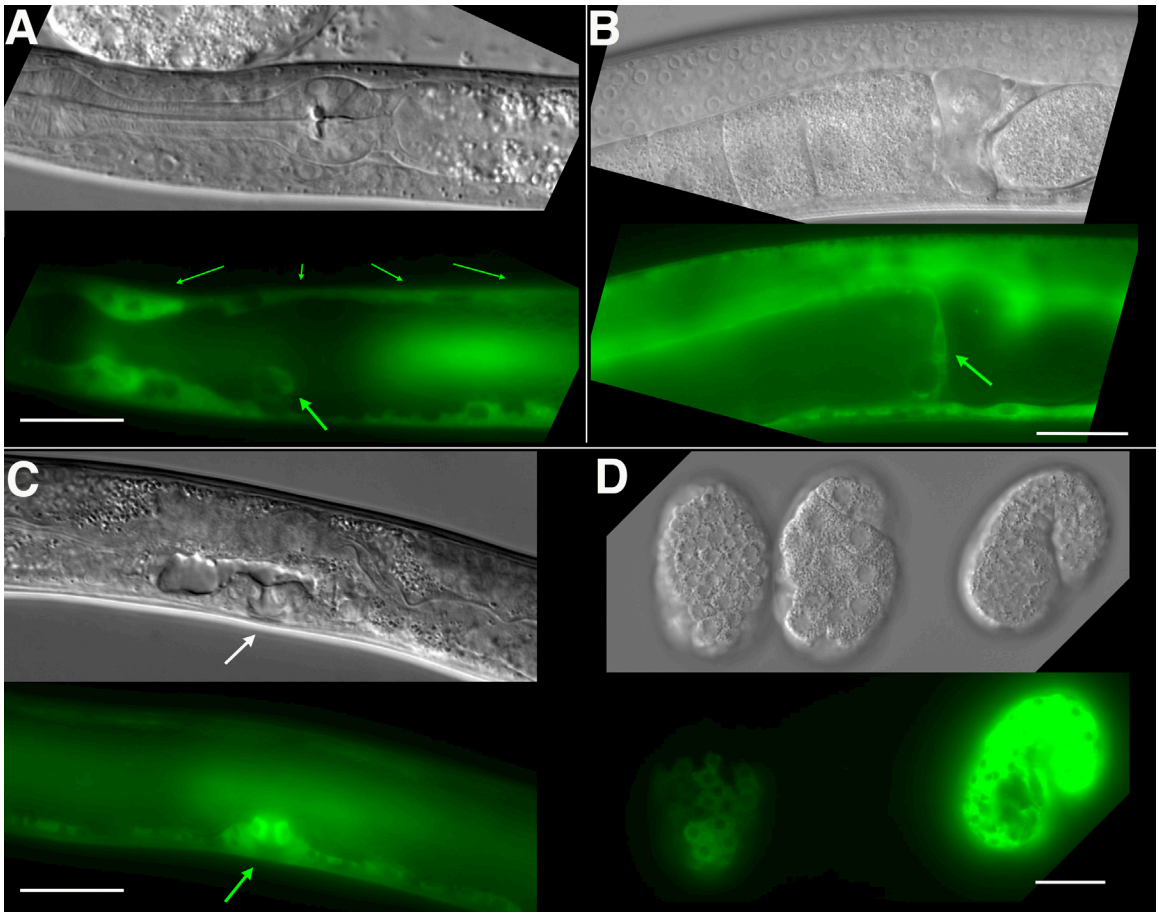

Figure 5

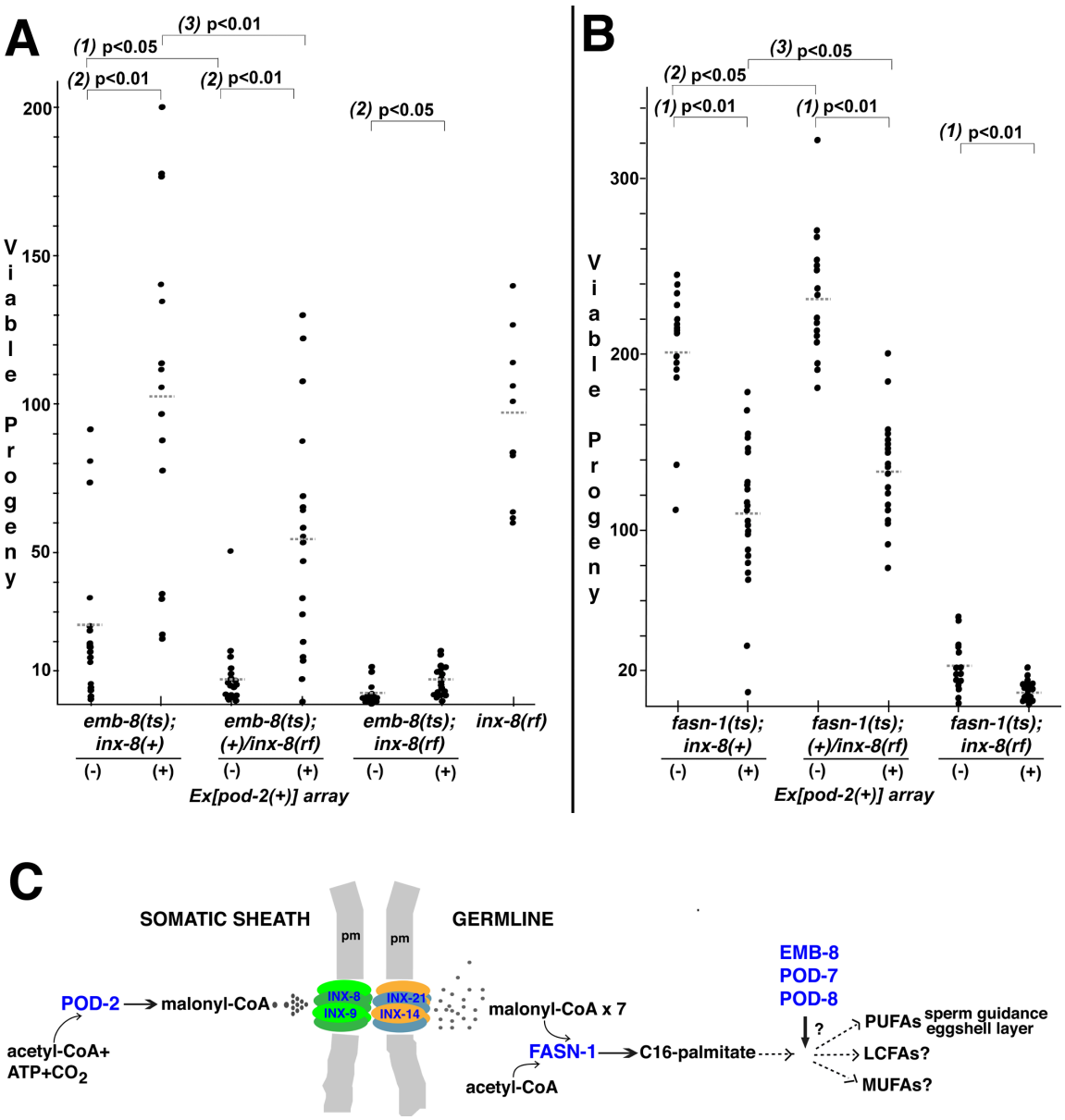
A
(3) p<0.01
(1) p<0.05
(2) p<0.01
(2) p<0.01
(2) p<0.05
Viable Progeny
200
150
100
50
10
emb-8(ts); inx-8(+)
emb-8(ts); (+)/inx-8(rf)
emb-8(ts); inx-8(rf)
inx-8(rf)
(-) (+) (-) (+) (-) (+)
Ex[pod-2(+)] array
B
(3) p<0.05
(2) p<0.05
(1) p<0.01
(1) p<0.01
(1) p<0.01
Viable Progeny
300
200
100
20
fasn-1(ts); inx-8(+)
fasn-1(ts); (+)/inx-8(rf)
fasn-1(ts); inx-8(rf)
(-) (+) (-) (+) (-) (+)
Ex[pod-2(+)] array
C
SOMATIC SHEATH
GERMLINE
pm
pm
INX-8
INX-9
INX-21
INX-14
POD-2
malonyl-CoA
acetyl-CoA+ ATP+CO2
malonyl-CoA x 7
FASN-1
acetyl-CoA
C16-palmitate
EMB-8
POD-7
POD-8
?
PUFAs
sperm guidance
eggshell layer
LCFAs?
MUFAs?

Figure 6

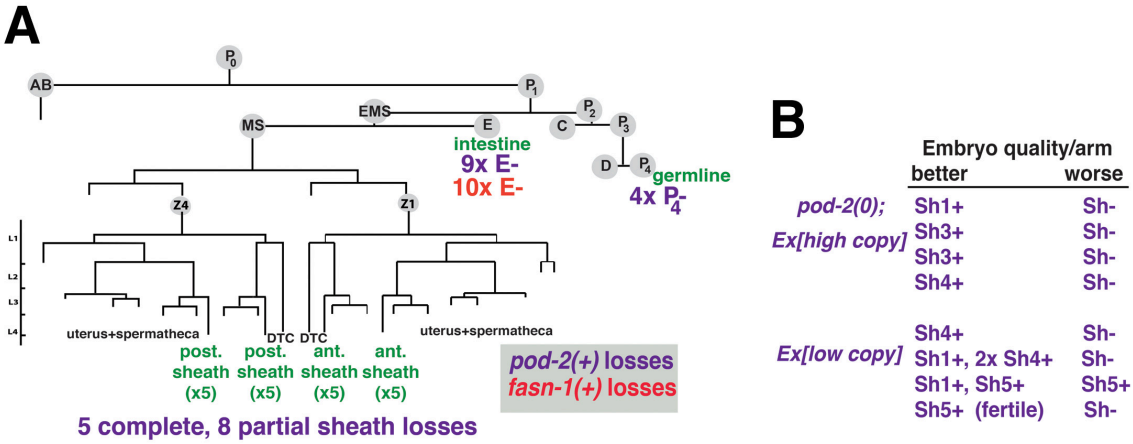
A
P0
AB
P1
EMS
MS
E
C
P2
P3
D
P4
intestine
9x E-
10x E-
germline
4x P4-
Z4
Z1
L1
L2
L3
L4
uterus+spermatheca
DTC DTC
uterus+spermatheca
post. sheath (x5)
post. sheath (x5)
ant. sheath (x5)
ant. sheath (x5)
pod-2(+) losses
fasn-1(+) losses
5 complete, 8 partial sheath losses
B
Embryo quality/arm
better
worse
pod-2(0);
Ex[high copy]
Sh1+
Sh3+
Sh3+
Sh4+
Sh-
Sh-
Sh-
Sh-
Ex[low copy]
Sh4+
Sh1+, 2x Sh4+
Sh1+, Sh5+
Sh5+ (fertile)
Sh-
Sh-
Sh5+
Sh-

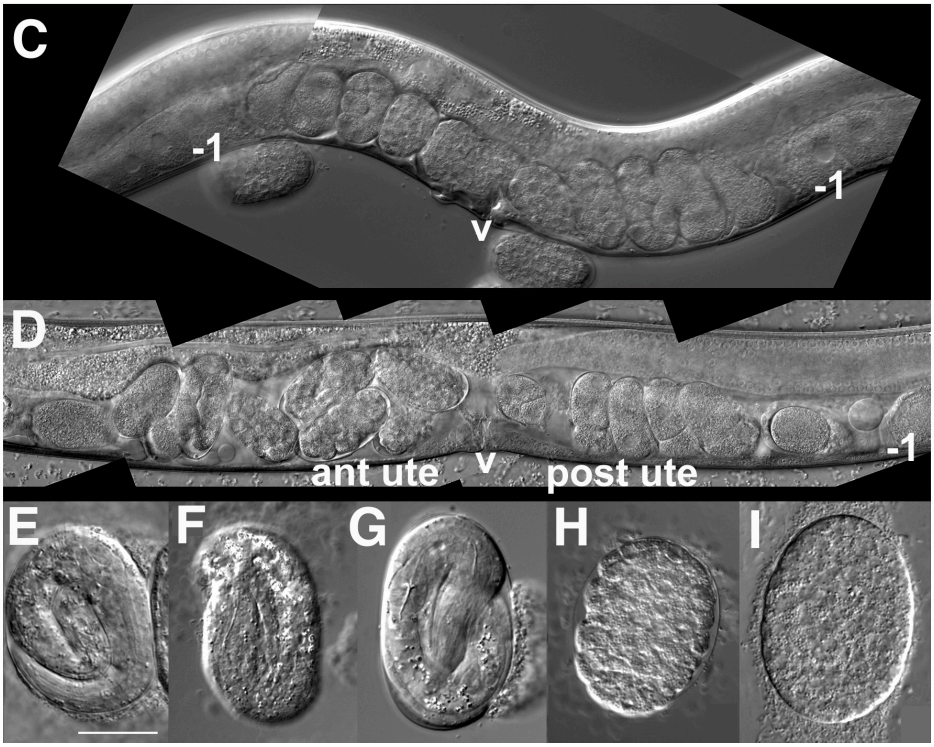
C
-1
-1
v
D
ant ute
v
post ute
-1
E
F
G
H
I

Figure 7

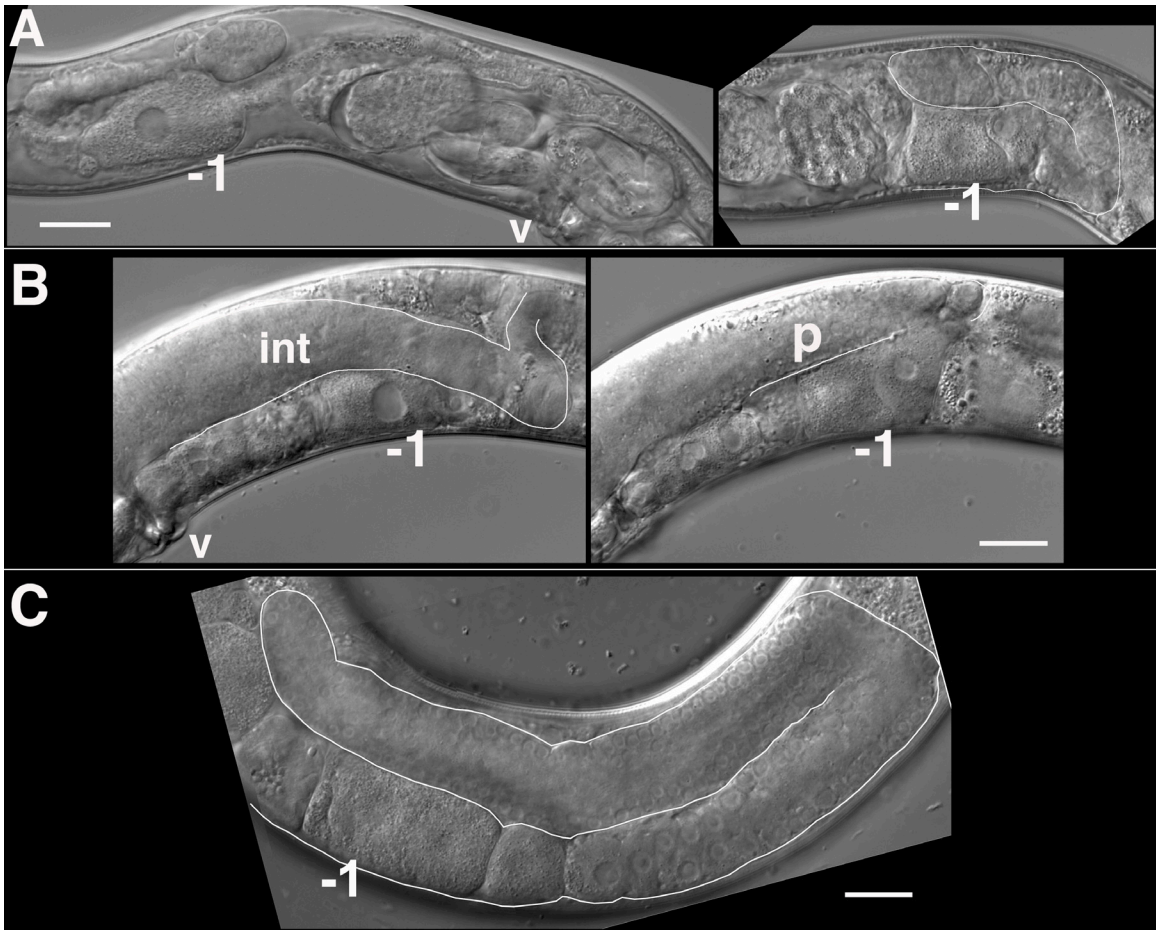

Figure 8

Figure 1–figure supplement table 1

***inx-8(rf)* exhibits reduced brood size and interacts with FA synthesis pathway genes**

Genotype	Brood size	Germ cells per gonad arm
20°C		
N2 (wild type)	291 ± 29 (n=33)	≥1000[1]
inx-8(rf)[2]	108 ± 40 (n=90)	322±18 (n=3; day 2 adult)
22°C		
inx-8(+)[3]	266 ± 40 (n=32)	
+/inx-8(rf)	255 ± 36 (n=32)	
fasn-1(g43ts); inx-8(+)	115 ± 41 (n=11)	
fasn-1(g43ts); +/ inx-8(rf)	114 ± 47 (n=11)	
fasn-1(g43ts); inx-8(rf)	4.5 ± 2.3 (n=12)	
emb-8(hc69ts); inx-8(+)	95 ± 50 (n=15)	
emb-8(hc69ts); +/inx-8(rf)	35 ± 37 (n=15)	
emb-8(hc69ts); inx-8(rf)	11 ± 9 (n=15)	

[1]*McCarter et al., 1997.*
[2]Full genotype *inx-8(tn1513 tn1555) inx-9(ok1502).* Approximately 4% of animals are infertile in one or both gonad arms (n=168).
[3]*inx-8(+)* provided on the balancer *mIs11* IV.
Source data 1. Brood size data for Figure 1–figure supplement table 1.

Figure 1–figure supplement table 2

Reduced soma-germline gap junction coupling delays gametogenesis

(a) *gfp::lin-41* expression at L4 vulval sub-stages

Genotype	L4.4	L4.5	L4.6	L4.7	L4.8	L4.9	L4.9< < molt
gfp::lin-41; inx-8(+)	1/11		3/3	5/6	5/6	4/4	
gfp::lin-41; inx-8(rf)		0/2	0/3	0/6		0/2	16/37
gfp::lin-41; inx-8/9(0); Ex[inx-8(DTC+,Sh-)]	0/11	0/3		0/2	0/1	0/3	6/14

(b) sperm appearance at L4 sub-stages

Genotype	L4.4	L4.5	L4.6	L4.7	L4.8	L4.9	L4.9< < molt
N2	0/9	0/2	0/5	4/11	1/2	1/2	6/6
inx-8(rf)	0/3		0/1	0/2	0/3	0/1	1/10

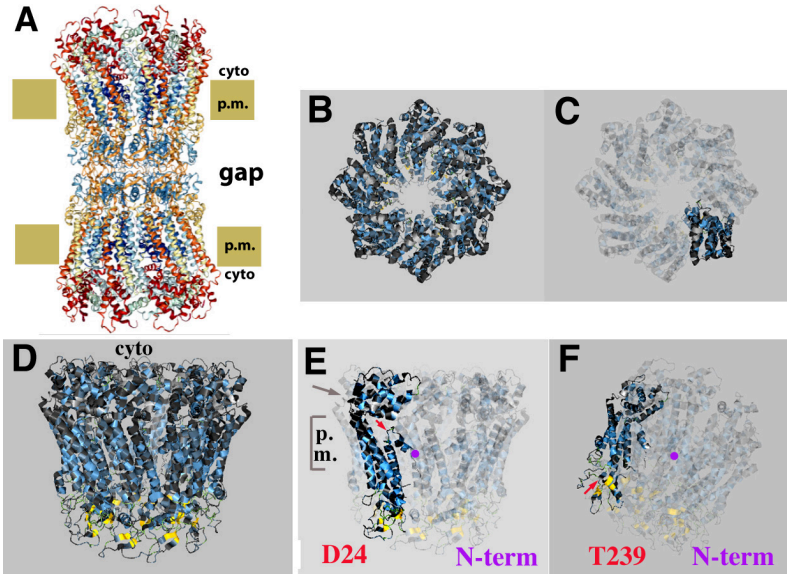

Figure 1–figure supplement 1

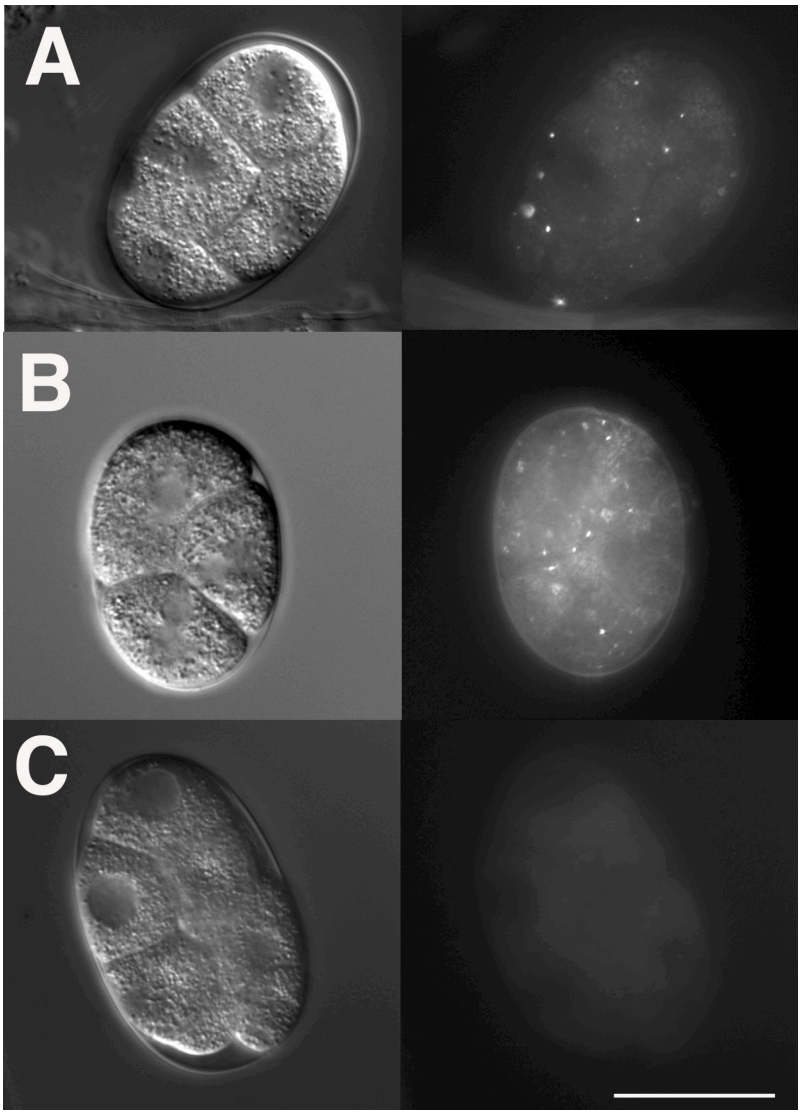

Figure 2–figure supplement 1

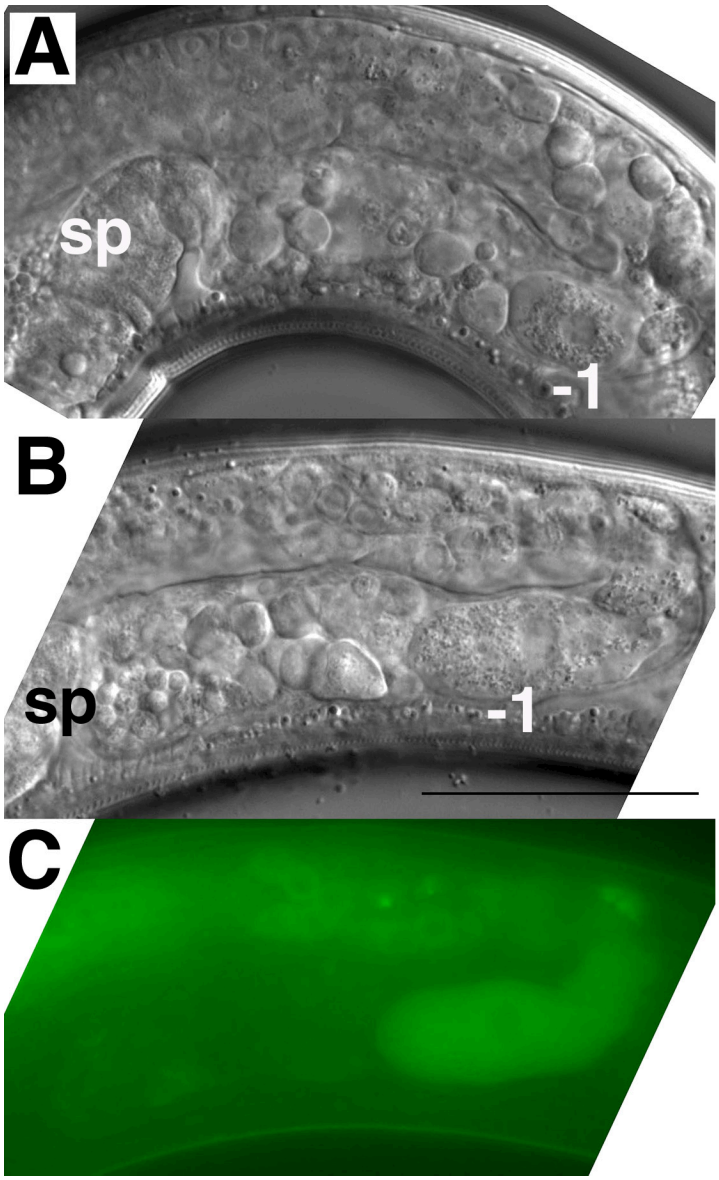

Figure 7–figure supplement 1

720 **Legends to Figure Supplements**

721 **Figure 1–figure supplement 1.** Predicted topological sites of amino acids
722 mutated in *inx-8(tn1513 tn1555) inx-9(0)*. (A) Atomic structure of the *C. elegans*
723 homomeric, homotypic INX-6 gap junction full channel, determined by *Oshima et*
724 *al., (2016)* (PDB I.D. 5H1R, rcsb.org (*Berman et al., 2000*), viewed with NGL
725 viewer (*Rose et al., 2018*). Octameric hemichannels associate via extracellular
726 loops to form an enclosed channel in the region classically identified by TEM as
727 the "gap" between closely aligned plasma membranes. cyto, cytoplasmic
728 membrane face; p.m., plasma membrane. (B-F) Model for INX-8 hemichannel
729 based on homology alignment to INX-6 (aquaria.ws). (B) Cytoplasmic view. (C)
730 Single subunit highlighted. In wild type this hemichannel is comprised of both
731 INX-8 and INX-9 subunits, and associates with germline hemichannels
732 comprised of INX-14+INX-21 or INX-14+INX-22. (D) Side view of hemichannel.
733 Beta-strands (yellow) in the extracellular loops contribute to walling off the pore.
734 (E) Single subunit highlighted. Kinked region (gray arrow) allows the cytoplasmic
735 structure of the subunits (cytoplasmic loop and C-terminus) to form a dome at the
736 pore entry. Amino termini (N-term) line the pore as a funnel; a loop in the amino
737 terminus allows for an interaction with residues in the dome (*Oshima et al.,*
738 *2016*). D24 in INX-8 (red arrow) lies near the D21 residue predicted by homology
739 with INX-6 (D25) to interact with the cytoplasmic dome. (F) INX-8 T239 is
740 predicted to lie adjacent to a beta-strand contributing to hemichannel-
741 hemichannel association (red arrow). (To expose the extracellular loop region in

742 relation to (E), the aspect of view is rotated towards the viewer and angled up to
743 the left.)
744
745 **Figure 2–figure supplement 1.** INX-8(rf)::GFP can be endocytosed by oocytes.
746 (A) *inx-8(+)::gfp* expressed in the somatic gonad sheath is endocytosed during
747 ovulation and appears as distinct fluorescent puncta in early embryos. (b) *inx-*
748 *8(rf)::gfp* expressed on an extrachromosomal array in *inx-8(0) inx-9(0)* animals is
749 endocytosed by ovulating oocytes. (c) *inx-8::gfp* expressed by the DTC in *inx-*
750 *8/9(0); Ex[inx-8(DTC+,Sh-)]* is not observed in early embryos. Bar, 20 µm.
751
752 **Figure 7–figure supplement 1.** Expression of *gfp::pod-2* in the germline fails to
753 rescue *inx-8(rf)* phenotypes. (**A**) Young (first-day) adult *inx-8(rf)* gonad arm. (B,
754 C) Young adult *inx-8(rf)* gonad arm expressing *mex-5p::gfp::pod-2::tbb-2-3'UTR*.
755 The *pod-2* isoform in this construct corresponds to *gfp::pod-2* isoform "a" in
756 *Figure 3B*. This isoform encompasses sequence homology to all of the
757 enzymatic sites in other ACC multi-functional enzymes. Sp, spermatheca; -1,
758 most proximal oocyte; bar, 50 µm.